THE JOURNAL OF BIOLOGICAL CHEMISTRY VOL. 287, NO. 11, pp. 8468–8483, March 9, 2012

Classically Activated Macrophages Use Stable Microtubules for Matrix Metalloproteinase-9 (MMP-9) Secretion*[S]

Received for publication, August 5, 2011, and in revised form, January 19, 2012 Published, JBC Papers in Press, January 23, 2012, DOI 10.1074/jbc.M111.290676

Raed Hanania[‡], He Song Sun[§], Kewei Xu[§], Sofia Pustylnik[§], Sujeeve Jeganathan[§], and Rene E. Harrison[§1]

From the [‡]Department of Cellular and Molecular Medicine, University of Ottawa, Ottawa, Ontario K1H 8M5, Canada and the [§]Department of Biological Sciences, University of Toronto Scarborough, Toronto, Ontario M1C 1A4, Canada

Background: Macrophages robustly secrete MMP-9 upon activation, and mechanisms for active delivery of MMP-9 vesicles to the cell surface have not been described.
Results: MMP-9 is packaged into unique ER protein-containing vesicles that associate with microtubule motors in activated macrophages.
Conclusion: Macrophage activation requires enhanced microtubule stabilization for rapid secretion of up-regulated MMP-9.
Significance: Understanding the nature and mechanisms of intracellular trafficking of MMP-9 is relevant to both immunology and cancer biology fields.

As major effector cells of the innate immune response, macrophages must adeptly migrate from blood to infected tissues. Endothelial transmigration is accomplished by matrix metalloproteinase (MMP)-induced degradation of basement membrane and extracellular matrix components. The classical activation of macrophages with LPS and IFN-γ causes enhanced microtubule (MT) stabilization and secretion of MMPs. Macrophages up-regulate MMP-9 expression and secretion upon immunological challenge and require its activity for migration during the inflammatory response. However, the dynamics of MMP-9 production and intracellular distribution as well as the mechanisms responsible for its trafficking are unknown. Using immunofluorescent imaging, we localized intracellular MMP-9 to small Golgi-derived cytoplasmic vesicles that contained calreticulin and protein-disulfide isomerase in activated RAW 264.7 macrophages. We demonstrated vesicular organelles of MMP-9 aligned along stable subsets of MTs and showed that selective modulation of MT dynamics contributes to the enhanced trafficking of MMP-9 extracellularly. We found a Rab3D-dependent association of MMP-9 vesicles with the molecular motor kinesin, whose association with the MT network was greatly enhanced after macrophage activation. Finally, we implicated kinesin 5B and 3B isoforms in the effective trafficking of MMP-9 extracellularly.

Macrophages are major effector cells of the innate immune response that are endowed with a specialized capacity for cell migration, phagocytosis of pathogens, and antigen presentation to T cells. Macrophages make up the predominant cell type in sites of inflammation after the neutrophils are spent (1). In order to carry out their function, it is important for macrophages to be able to migrate from blood, where they circulate as monocytes, to target tissues. Following endothelial transmigration, they must transverse the subendothelial basement membrane and the interstitial matrix composed mainly of collagen. This is largely accomplished by matrix metalloproteinase (MMP)[2]-induced degradation of basement membrane and extracellular matrix components (2).

During an inflammatory response, macrophages may become activated from exposure to various signals. Macrophage classical activation is induced by exposure to interferon-γ (IFN-γ), a proinflammatory cytokine produced by the host, either alone or in conjunction with pathogenic stimuli, such as lipopolysaccharide (LPS) (3). Classically activated macrophages, also called M1 macrophages, demonstrate increased cell spreading, enhanced phagocytosis, and antigen presentation capacities and amplified inducible nitric-oxide synthetase expression for the production of nitric oxide (2, 4–7). Additionally, classical activation results in the enhanced production and secretion of MMPs to the cell exterior (2) as well as increased levels of stabilized cytoplasmic microtubules (MTs) (4, 8, 9).

The MT cytoskeleton plays many important roles in cell function, such as migration, phagocytosis of pathogens, and antigen presentation (8, 10–12). The MT cytoskeleton alternates between elongation and shrinkage phases in a process termed "dynamic instability" (13, 14). Association of proteins such as MAP4 with MTs results in their enhanced stability (15). As a result of their longevity, stable MTs accumulate post-translational modifications, such as the acetylation of α-tubulin on its lysine 40 residue (16). Therefore, subsets of stabilized MTs can be identified by the presence of acetylated α-tubulin subunits and are biochemically distinct from their dynamic counterparts (16–18).

Of particular importance to cell migration is MMP-9 secretion due to its ability to degrade extracellular matrix compo-

* This work was supported by Canadian Institutes of Health Research (CIHR) Grant MOP-68992 (to R. E. H.).
[S] This article contains supplemental Figs. 1 and 2.
[1] Recipient of a CIHR New Investigator Award and an Ontario Early Researcher Award. To whom correspondence should be addressed. Tel.: 416-287-7377; Fax: 416-287-7676; E-mail: harrison@utsc.utoronto.ca.

[2] The abbreviations used are: MMP, matrix metalloproteinase; BMDM, bone marrow-derived macrophage; BFA, brefeldin A; LC3, light chain 3; LAMP, lysosomal associated membrane protein; MT, microtubule; PDI, protein-disulfide isomerase; TIMP, tissue inhibitor of metalloproteinases; IP, immunoprecipitation; ER, endoplasmic reticulum; TPEN, *N*,*N*,*N*′,*N*′-tetrakis(2-pyridylmethyl)ethylenediamine.

nents, such as collagens and elastins (19). MMP-9 expression is typically absent or minimal in normal tissues and is greatly enhanced during inflammation and wound healing (20). Macrophages do not constitutively express MMP-9; rather, LPS exposure has been shown to induce MMP-9 gene expression as well as increase the amount of biologically active MMP-9 in the cell culture supernatant (21). Although MMP activity is strongly regulated at the transcriptional level, MMP function is managed by recruitment of MMPs to the cell surface, where they are secreted as inactive zymogens (pro-MMPs) (22). Pro-MMP-9 activation is achieved by the action of extracellular proteases, such as plasmin (23); other MMPs, such as MMP-3 (24), MMP-7 (25), and MMP-13 (26); and LPS-associated serine proteinases (19). Upon activation, MMP-9 is converted from a 92-kDa zymogen form to an 82-kDa active form (22). Further regulation of MMP-9 activity is offered by its natural inhibitor *in vivo*, the tissue inhibitor of metalloproteinase-1 (TIMP-1) (27).

MMP-9 plays a critical role in mediating cell migration. Blocking of MMP-9 by monoclonal antibodies inhibits the migration of bone marrow stem cells into the circulation (28), and MMP-9 has been shown to assist in monocyte migration (29, 30). Additionally, a role for MMP-9 in macrophage migration during the inflammatory response was demonstrated *in vivo*, where inhibition of MMP-9 activation resulted in the abolished ability of macrophages to migrate to the elicited site of inflammation (23). The mechanisms involved in regulating MMP-9 expression, as well as its extracellular activation and inhibition, have been extensively characterized (31). Although MMP-9 dependence was demonstrated for macrophage migration (23), the dynamics of MMP-9 production and intracellular distribution after its expression as well as the mechanisms involved in its trafficking before its secretion remain uncharacterized. In the present work, we localized intracellular MMP-9 to distinct cytoplasmic vesicles in macrophages stimulated with LPS and IFN-γ that were distinct from neutrophil zymogen granules. MMP-9 was instead packaged into unique vesicles that contained the normally ER-resident proteins, calreticulin and protein-disulfide isomerase (PDI). We established a functional contribution of stable MTs in activated macrophages for the enhanced trafficking of MMP-9 extracellularly. Finally, we showed a Rab3D-dependent association of the molecular motor kinesin with MMP-9 vesicles and implicated both kinesin 5B and 3B isoforms in mediating MMP-9 trafficking.

EXPERIMENTAL PROCEDURES

Reagents and Antibodies—Dulbecco's modified Eagle's medium (DMEM) and fetal bovine serum (FBS) were purchased from Wisent Inc. (St-Bruno, Canada). LPS from *Salmonella enterica* serotype Typhimurium, IFN-γ, TPEN, nocodazole, and taxol were from Sigma-Aldrich Inc. Brefeldin A (BFA) from *Penicillium brefeldianum*, Alexa Fluor® phalloidin, and 4′,6-diamidino-2-phenylindole (DAPI) were obtained from Invitrogen. FuGENE HD was purchased from Roche Applied Science. Antibodies were obtained as follows. Rabbit polyclonal anti-MMP-9, rat polyclonal anti-CD11b (Mac-1), and mouse monoclonal anti-PDI were from Abcam Inc. (Cambridge, MA). Mouse monoclonal anti-β-actin, anti-α-tubulin, and anti-acetylated tubulin were obtained from Sigma-Aldrich. Mouse monoclonal anti-MAP4 and anti-GM130 were from BD Transduction Laboratories (San Jose, CA). Mouse monoclonal (SUK4) anti-kinesin and rat polyclonal (ID4B) anti-lysosome-associated membrane protein-1 (LAMP-1) were purchased from the Developmental Studies Hybridoma Bank. Mouse monoclonal anti-ubiquitinylated protein antibody was from Enzo® Life Sciences (Plymouth, PA). Mouse monoclonal anti-Rab27a was from Santa Cruz Biotechnology, Inc. (Santa Cruz, CA). Mouse monoclonal anti-KDEL was from Stressgen® (Ann Arbor, MI). Cy™2-, Cy™3-, and Cy™5-conjugated AffiniPure donkey anti-rat, -goat, -rabbit, and -mouse IgG and peroxidase-conjugated AffiniPure donkey anti-rabbit and -mouse IgG were from Jackson ImmunoResearch Laboratories (West Grove, PA).

Cell Culture, Transfection, and Mouse Macrophage Isolation—The murine RAW 264.7 macrophage cell line was obtained from the American Type Culture Collection (Manassas, VA) and maintained at 37 °C supplied with 5% CO_2 in DMEM supplemented with 10% heat-inactivated FBS. For all experiments, RAW 264.7 cells were grown to 60–80% confluence in tissue culture 6-well plates, with or without 25-mm glass coverslips. RAW 264.7 cells were transiently transfected using FuGENE HD according to the manufacturer's instructions, with overnight incubations for plasmid expression. Primary bone marrow-derived macrophages (BMDMs) were harvested from the femoral bones of C57BL/6 mice. Briefly, femoral bones were separated from surrounding tissues and cut on both ends. BMDMs were obtained by femoral lavage with DMEM containing 10% heat-inactivated FBS, supplemented with penicillin and streptomycin (100 IU/ml and 100 μg/ml, respectively). Cells were grown in tissue culture 6-well plates at 37 °C with 5% CO_2 for 5 days to allow for differentiation into macrophages.

Macrophage Activation and Pharmacological Treatments—Resting RAW 264.7 cells or differentiated murine BMDMs were classically activated by a combination of 0.1 μg/ml LPS and 100 units/ml IFN-γ for 9 h, unless indicated otherwise, in FBS-free DMEM. Inhibition of protein traffic from the ER to the Golgi apparatus was performed by incubating RAW 264.7 cells with 5 μg/ml BFA for 9 h during classical activation. For zinc chelation experiments, cells were incubated with 1.5 μM TPEN for 9 h during activation. For depolymerization of the MT cytoskeleton, RAW 264.7 cells were classically activated and treated with 10 μM nocodazole in the last 3 h of activation. Enhanced MT stabilization was achieved by incubating classically activated RAW 264.7 cells with 0.1 μM taxol or 0.1 μM nocodazole in the last 1 or 3 h of activation, respectively.

Gelatin Zymography, Western Blot, and Densitometric Analysis—Cell culture supernatants were collected and total cell lysates were obtained by scraping cells in radioimmune precipitation assay lysis buffer in the presence of protease and phosphatase inhibitor mixtures (Sigma-Aldrich). For gelatin zymography, protein samples were mixed in Laemmli buffer lacking 2-mercaptoethanol and incubated at room temperature for 15 min. Equal amount of protein was loaded and separated on 8% SDS-PAGE containing 0.1% gelatin from bovine skin, type B (Sigma-Aldrich). After electrophoresis, gels were washed three times for 20 min in zymogram wash buffer (2.5%

Triton X-100, 50 mM Tris-HCl, pH 7.5) and incubated overnight at 37 °C in zymogram developing buffer (50 mM Tris-HCl, pH 7.5, 10 mM $CaCl_2$, 5 μM $ZnCl_2$, 150 mM NaCl). Gels were then stained with 0.25% Coomassie Brilliant Blue R-250 (Bio-Rad) for 6 h and destained twice for 30 min in 7% acetic acid, 40% methanol solution. Gelatinolytic activity appeared as a clear band on a dark background. For Western blotting, protein samples were dissolved in Laemmli buffer and boiled for 10 min. An equal amount of protein was separated on 8 or 10% SDS-PAGE and transferred to nitrocellulose membranes (Bio-Rad). Blots were blocked for 1 h in 5% skim milk, TBST (Bio-Shop Canada Inc., Burlington, Canada) and then incubated with the corresponding primary antibody overnight at 4 °C. The dilutions were as follows: MMP-9 (1:1000), acetylated α-tubulin (1:2000), α-tubulin (1:2000), β-actin (1:2000), KIF5B (1:500). Blots were incubated with the relevant peroxidase-coupled secondary antibody (1:1000) for 1 h, and bound antibody was visualized using the Supersignal® West Pico chemiluminescent substrate kit (Pierce), according to the manufacturer's instructions. Protein bands were measured by densitometry scanning of independent experiments using ImageJ software (National Institutes of Health, Bethesda, MD) to determine the relative -fold increases of pixel intensities compared with resting or activated cell culture supernatants or lysates. Protein bands subjected to densitometric analysis were not saturated or overexposed.

Immunoprecipitation—Control and activated cells were washed twice with ice-cold PBS, and protein lysates were obtained using radioimmune precipitation assay buffer. Total proteins (150 μg) were precleared overnight with rotation at 4 °C using 50 μl of Protein A/G Plus-agarose (sc-2003, Santa Cruz Biotechnology, Inc.). Total protein concentration from precleared lysates was then quantified. Immunoprecipitates were collected by incubating 40 μl of the IP matrix ExactaCruz B (sc-45039, Santa Cruz Biotechnology, Inc.) with 1 μg of kinesin 5B antibody (K1014, Sigma) or 40 μl of the IP matrix ExactaCruz C (sc-45040, Santa Cruz Biotechnology, Inc.) with 1 μg of tubulin antibody (T9026, Sigma). An equivalent amount of isotypic IgG (Sigma) was bound to the ExactaCruz B and C IP matrices as negative controls. Precleared lysates and IP antibody-IP matrix complexes were incubated overnight with rotation at 4 °C. Pelleted matrices were washed twice with 500 μl of ice-cold PBS, and proteins were eluted using reducing 2× electrophoresis sample buffer. Samples were resolved by SDS-PAGE and analyzed by Western blotting.

Immunostaining and Fluorescent Imaging—Cells were fixed in 4% PFA for 20 min and permeabilized with 0.1% Triton X-100 in PBS containing 100 mM glycine for 20 min. For immunostaining of kinesin, cells were fixed and permeabilized in ice-cold 100% methanol for 10 min at −20 °C. Cells were blocked in 5% FBS, PBS for 1 h and incubated with the indicated primary antibodies in 1% FBS, PBS for 1 h using the following dilutions: MMP-9 (1:1000), acetylated α-tubulin (1:5000), MAP4 (1:500), α-tubulin (1:10000), PDI (1:200), GM130 (1:200), LAMP-1 (1:4), ubiquitinylated proteins (1:1000), KDEL (1:200), calreticulin (1:200), Mac-1 (1:1000), Rab27a (1:200), and kinesin (1:100). Cells were then incubated with the corresponding fluorochrome-conjugated secondary antibodies (1:1000) in 1% FBS, PBS for 1 h. Where indicated, secondary antibodies were incubated together with Alexa Fluor® phalloidin (1:500) to stain for the actin cytoskeleton. Cells were mounted using Dako Fluorescent Mounting Medium (DakoCytomation, Carpinteria, CA). For nuclear staining, cells were washed twice with double-distilled H_2O and incubated for 10 min with DAPI (1:10,000) before mounting.

For triple immunolabeling of MMP-9, acetylated α-tubulin or MAP4, and α-tubulin, cells were paraformaldehyde-fixed, permeabilized, and blocked as before. Briefly, the cells were incubated with primary antibodies to MMP-9 and acetylated α-tubulin or MAP4, followed by incubation with the appropriate fluorochrome-conjugated secondary antibodies. The cells were then blocked in 5% FBS, PBS for 1 h and then incubated with primary antibody to α-tubulin, followed by incubation with the relevant fluorochrome-conjugated secondary antibody.

Cells were visualized under a ×63/1.4 numerical aperture oil immersion objective using an inverted Zeiss AxioObserver.Z1 epifluorescent microscope using Axiovision software or with an upright Zeiss LSM510 confocal microscope using the ZEN software (Zeiss, Thornwood, NY). Total internal reflection microscopy was performed using an inverted Zeiss AxioVert 200 M epifluorescent microscope equipped with an α-Plan-Fluor ×100/1.45 numerical aperture objective.

Quantifications and Statistical Analysis—RAW 264.7 cells were classically activated, fixed, and immunostained for endogenous MMP-9 and imaged by epifluorescence. The number of MMP-9 vesicles showing co-recruitment with the indicated proteins was tabulated for 100 MMP-9 vesicles and averaged. The indicated proteins were considered positively recruited to MMP-9 vesicles if they demonstrated the same punctate staining that exactly colocalized with MMP-9. For quantification of the total intracellular fluorescence intensity of MMP-9, the intensity of 100 individual cells was measured using NIH ImageJ software for each group. Images were acquired using the same fluorescence intensity and exposure time between treatments and replicates. The average relative -fold increase of pixel intensities was calculated compared with that of activated cells and normalized for background fluorescence observed in resting cells. Quantitative colocalization analysis was performed on 10 images of the indicated proteins with MMP-9 using Zeiss ZEN software to measure Pearson's coefficients. To determine the average number of MMP-9 vesicles per activated macrophage cell expressing either KIF5B or KIF3B rigor mutants, the number of discrete MMP-9 vesicles in each cell was tabulated for 15 macrophages and averaged.

Experimental values are presented as mean ± S.E. of the experimental triplicates. Microsoft Excel was used to perform Student's *t* test evaluations of the data, with values of $p < 0.05$ considered significant.

RESULTS

Analysis of Intracellular and Extracellular Levels of MMP-9 in Classically Activated RAW 264.7 Cells—Macrophages stimulated with LPS exhibit a time-dependent increase in MMP-9 expression and secretion (21). However, the analysis of MMP-9 levels in macrophages classically activated with both LPS and IFN-γ remains poorly resolved. We therefore examined both

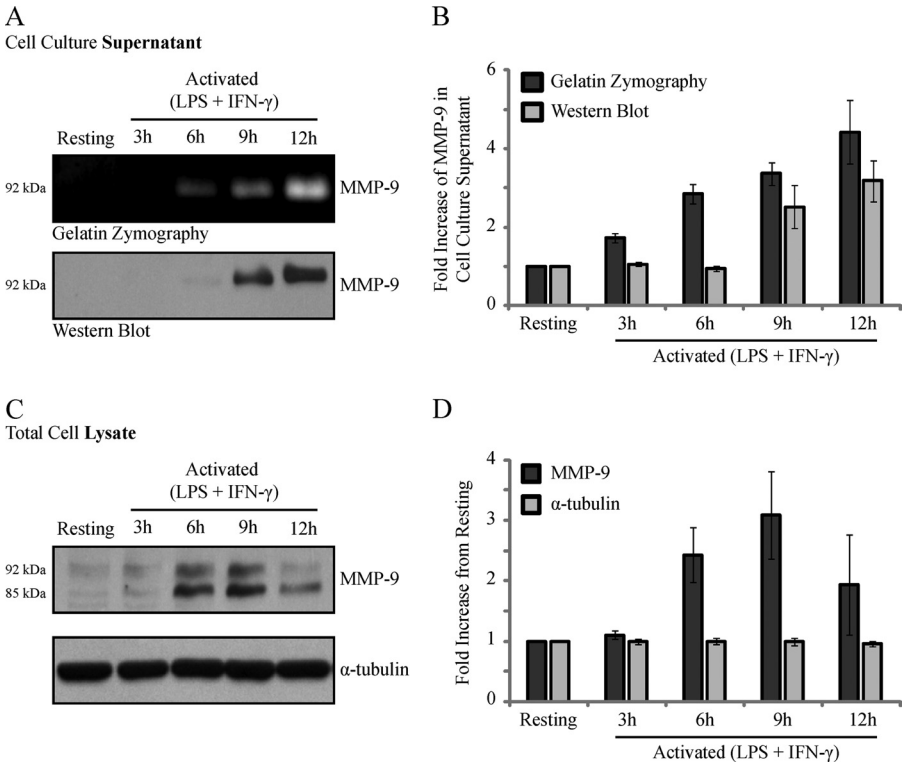

FIGURE 1. **Analysis of MMP-9 levels in the cell culture supernatants and total cell lysates of resting and LPS/IFN-γ-activated RAW 264.7 cells.** RAW 264.7 cells were stimulated with LPS/IFN-γ for 3, 6, 9, and 12 h or left unstimulated. After the indicated time points, the cell culture supernatants were collected, and the cells were lysed and subjected to gelatin zymography or immunoblotting. Shown are the gelatin zymogram and immunoblot (*A*) and densitometric analysis (*B*) of macrophage cell culture supernatants for secreted MMP-9. Also shown are Western blot (*C*) and densitometric analysis (*D*) of macrophage total cell lysates for levels of intracellular MMP-9 and α-tubulin, used as a loading control. *Error bars*, S.E.

the intracellular and extracellular levels of MMP-9 in resting or LPS/IFN-γ (0.1 μg/ml and 100 units/ml, respectively)-activated RAW 264.7 cells for 3, 6, 9, or 12 h (Fig. 1). MMP-9 was detected in the cell culture supernatant at 6 h after activation by gelatin zymography (Fig. 1*A*, *top*) and at 9 h after activation by Western blotting (Fig. 1*A*, *bottom*). Densitometric analysis of MMP-9 immunoblots demonstrated a steady increase of extracellular MMP-9 levels over time (Fig. 1*B*). It is important to note that only the zymogen 92-kDa form of MMP-9 was detected. The absence of the active 82-kDa form in the cell culture supernatant may be a result of culture conditions, in which MMP-9 is diluted away from its activators in the medium (22). Although gelatin zymography is a common tool used to assess the levels of gelatinases (32), to measure the amount of secreted and intracellular MMP-9 protein levels, we next turned to immunoblotting. Western blot analysis of MMP-9 in the total cell lysate consistently revealed two bands of apparent molecular masses of 85 and 92 kDa (Fig. 1*C*). It was previously shown that the 85 kDa band represents an underglycosylated precursor form of MMP-9 found intracellularly, whereas the 92 kDa band represents a fully glycosylated mature form that is secreted into the extracellular space (33). Densitometric analysis was performed on the 92 kDa band without consideration for the 85 kDa band (Fig. 1*D*) because we were interested in studying the trafficking of the mature protein that is detected extracellularly. Classically activated RAW 264.7 cells exhibited an increase in MMP-9 protein production over time, with the largest amount of intracellular MMP-9 obtained at 9 h after activation, followed by a drop in levels at 12 h (Fig. 1*D*). Because we did not detect the active form of MMP-9 (82 kDa) in the cell culture supernatant, and because we will not be considering the precursor form (85 kDa) in the cell lysate, the term "MMP-9" will be used herein to describe the 92-kDa zymogen detected both intracellularly and extracellularly.

MMP-9 Is Processed through Biosynthetic Pathway and Packaged into Discrete Golgi-derived Vesicles—The intracellular nature of MMP-9 in macrophage cells remains uncharacterized. To begin, RAW 264.7 cells were immunostained for MMP-9 and GM130 and imaged by epifluorescent microscopy (Fig. 2). As expected, resting RAW 264.7 cells did not demonstrate any detectable intracellular MMP-9 (Fig. 2*A*). In contrast, RAW 264.7 cells activated with LPS/IFN-γ revealed MMP-9 staining that localized to the Golgi as well as to discrete vesicular structures outside of the Golgi (Fig. 2*B*). To see if these discrete MMP-9-containing vesicles were a general characteristic of macrophages, we also examined primary mouse BMDMs. Unstimulated cells showed no MMP-9 content (not shown), whereas LPS/IFN-γ-activated BMDMs revealed pronounced vesicles reactive for MMP-9 antibodies (Fig. 2*C*).

In general, secreted proteins are transported from the ER to the Golgi and subsequently to the plasma membrane (34). Because we observed MMP-9 staining that localized to the Golgi apparatus, we wanted to follow MMP-9 through this paradigm of protein transport and verify its Golgi-derived nature. To do this, RAW 264.7 cells were activated in the presence of BFA, a potent inhibitor of protein delivery from the ER to the

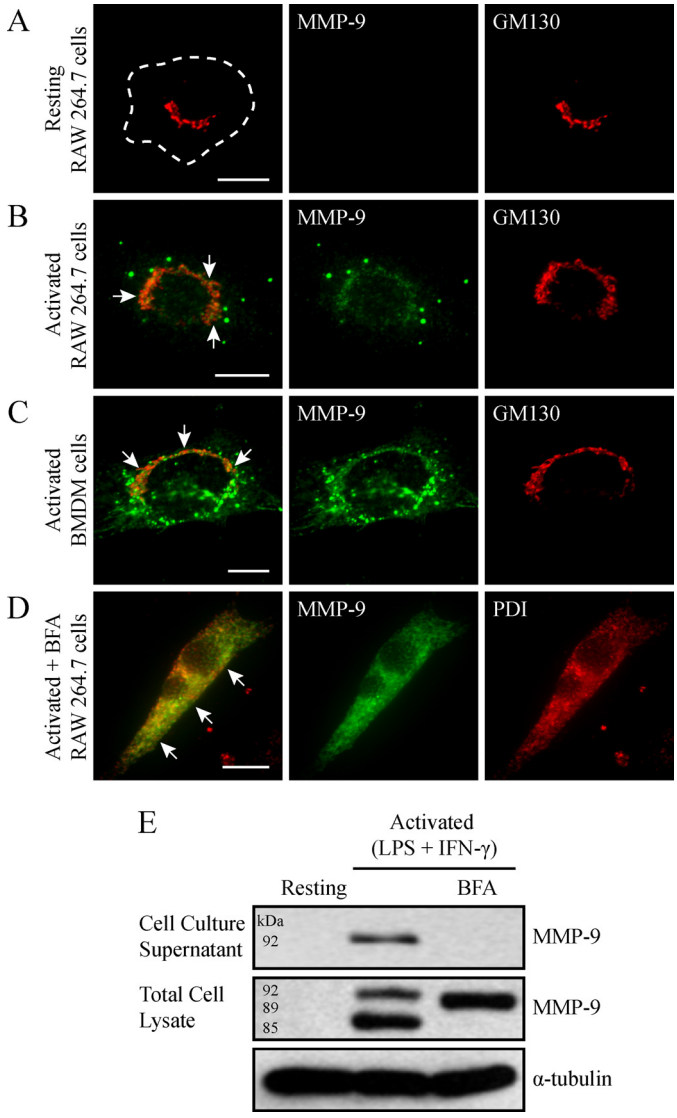

FIGURE 2. **MMP-9 is sorted into discrete Golgi-derived vesicles.** Resting RAW 264.7 cells were fixed, immunostained for endogenous MMP-9, and imaged by epifluorescent microscopy (*A*). Alternatively, RAW 264.7 cells (*B*) and BMDM cells (*C*) were activated with LPS/IFN-γ (0.1 μg/ml and 100 units/ml, respectively, for 9 h), fixed, immunostained for MMP-9 (*green*) and GM130 (*red*), and imaged by epifluorescence. Note that images displayed are of cells containing higher than usual numbers of MMP-9 vesicles and may not be representative of the average number of MMP-9 vesicles per activated macrophage. *Scale bars*, 10 μm. The *arrows* indicate colocalization of MMP-9 with GM130. To inhibit ER to Golgi transport, RAW 264.7 cells were activated (0.1 μg/ml LPS and 100 units/ml IFN-γ for 9 h) in the presence of 5 μg/ml BFA. Cells were fixed and analyzed for MMP-9 (*green*) and PDI (*red*) by immunofluorescence (*D*). *Scale bar*, 10 μm. The *arrows* indicate colocalization between MMP-9 and PDI. Alternatively, the cell culture supernatants were collected, and the cells were lysed and subjected to immunoblotting for MMP-9 and α-tubulin (*E*).

Golgi apparatus (35). Epifluorescent imaging of cells immunostained for MMP-9 and the ER marker PDI revealed an accumulation of MMP-9 in the ER (Fig. 2*D*). To determine the effects of blocking ER-to-Golgi transport on MMP-9 production and secretion, immunoblotting for MMP-9 was performed on the cell culture supernatant and total cell lysate of resting and activated cells treated with BFA or not. Compared with activated cells, activated/BFA-treated cells did not show MMP-9 in the cell culture supernatant (Fig. 2*E*), indicating that BFA successfully halted its secretion. Additionally, the lysates of BFA-treated cells revealed an intermediate form of MMP-9, with an apparent molecular mass of 89 kDa, and lacked the underglycosylated (85-kDa) or fully glycosylated (92-kDa) forms present in untreated activated macrophages (Fig. 2*E*). This intermediate may reflect a transient, immature form of MMP-9 that has been glycosylated in the ER and is missing glycosylation in the Golgi. Altogether, these results demonstrate that MMP-9 maturation requires processing in the ER as well as Golgi compartments, after which it is packaged into discrete vesicles.

MMP-9 Vesicles in Macrophages Are Distinct from Neutrophil Tertiary Granules—Unlike macrophages, neutrophils produce MMP-9 in the absence of immunological challenge, where it is stored in tertiary granules (36). These tertiary granules have undergone extensive characterization (37); however, the identity of vesicles transporting MMP-9 in macrophages is unknown. We therefore sought to characterize the composition of the MMP-9-containing vesicular structures that we observed in activated macrophages. To begin, we wanted to determine if macrophage MMP-9 vesicles have a similar composition as neutrophil tertiary granules. It is well established that Rab27a, a GTPase involved in specialized vesicle trafficking, colocalizes with MMP-9 and regulates its secretion in neutrophils (38). To test for a similar role in macrophages, we immunostained activated cells for endogenous Rab27a and MMP-9. Epifluorescent imaging of these cells revealed a differential sorting of Rab27a and MMP-9 into separate vesicular subpopulations (Fig. 3*A*), where only 0.83 ± 0.6% of MMP-9 vesicles were Rab27a-positive (Fig. 3*D*). In addition to Rab27a, neutrophils pack the adhesion molecule Mac-1 in tertiary granules (37). Immunostaining of Mac-1 and MMP-9 in activated RAW 264.7 cells showed a general absence of Mac-1 recruitment to MMP-9 vesicles (Fig. 3*B*), where only 0.67 ± 0.3% of MMP-9 vesicles were Mac-1-positive (Fig. 3*D*). We also investigated the possible localization of CD63 to macrophage MMP-9 vesicles. Although CD63 is found predominantly in primary granules, it has been shown to also colocalize with Mac-1 in neutrophils (39) and to associate with the membranes of macrophage phagolysosomes, secretory granules, and multivesicular bodies (40). RAW 264.7 cells expressing GFP-tagged CD63 were activated and immunostained for endogenous MMP-9 (Fig. 3*C*). Epifluorescent imaging of these cells revealed that only 1.2 ± 0.4% of MMP-9 vesicles demonstrated CD63 recruitment (Fig. 3*D*). In summary, these results indicated that the composition of MMP-9 vesicles in activated macrophages is different from MMP-9 granules in neutrophils.

MMP-9 Is Sorted into Calreticulin- and PDI-containing Transport Vesicles—We showed that activated macrophages distribute MMP-9 into vesicles that differ in composition from neutrophil tertiary granules. It was previously demonstrated that cells deficient in calreticulin, an ER calcium-binding protein and chaperone, possess decreased MMP-9 levels and activity (41). We therefore wanted to determine if calreticulin associated with MMP-9 in activated macrophages. Epifluorescent imaging of cells immunostained for endogenous calreticulin and MMP-9 showed concentrated calreticulin enrichment in 98.3 ± 0.7% of MMP-9 vesicles as well as diffuse calreticulin

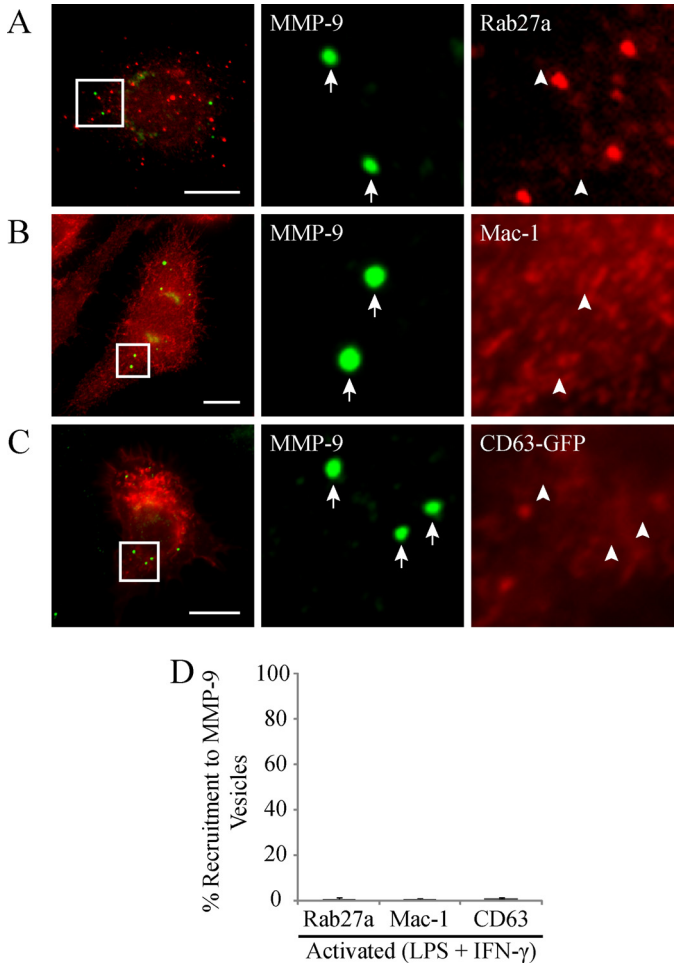

FIGURE 3. **MMP-9 vesicles do not colocalize with Rab27a, Mac-1, and CD63.** LPS/IFN-γ (0.1 μg/ml and 100 units/ml, respectively, for 9 h)-activated RAW 264.7 cells were analyzed for Rab27a (*A*), Mac-1 (*B*), or expressed CD63-GFP (*C*) (all shown in *red*) and MMP-9 (*green*), by epifluorescence. The *arrows* identify MMP-9 vesicles, whereas *arrowheads* indicate the absence of co-recruitment to MMP-9 vesicles. *Scale bars*, 10 μm. The percentage of MMP-9 vesicles showing co-recruitment with the indicated markers was quantified (*D*).

staining localized to the ER (Fig. 4, *A* and *F*). We next wanted to determine if calreticulin was the only ER protein that localized to MMP-9 vesicles. Immunostaining and epifluorescent imaging of activated RAW 264.7 cells also showed concentrated staining of PDI in 98.7 ± 0.9% of MMP-9 vesicles (Fig. 4, *B* and *F*). These results led us to investigate the possibility that the MMP-9 punctate structures we observed may actually be dilated pockets within the ER because calreticulin and PDI are ER-resident proteins (42, 43). ER-resident proteins are targeted and retained in the ER via a KDEL signal peptide. This sequence is thus found throughout the ER, on ER proteins that leak out toward the Golgi, and on recycling vesicles from the Golgi back to the ER (44–46). Immunostaining and epifluorescent imaging of activated RAW 264.7 cells revealed that MMP-9 vesicles were devoid of this KDEL sequence (Fig. 4*C*). Only 0.67 ± 0.3% of MMP-9 vesicles were KDEL-positive (Fig. 4*F*). These data indicate that the MMP-9 vesicles are not contained within the ER and are probably not transport or recycling vesicles between the ER and Golgi apparatus.

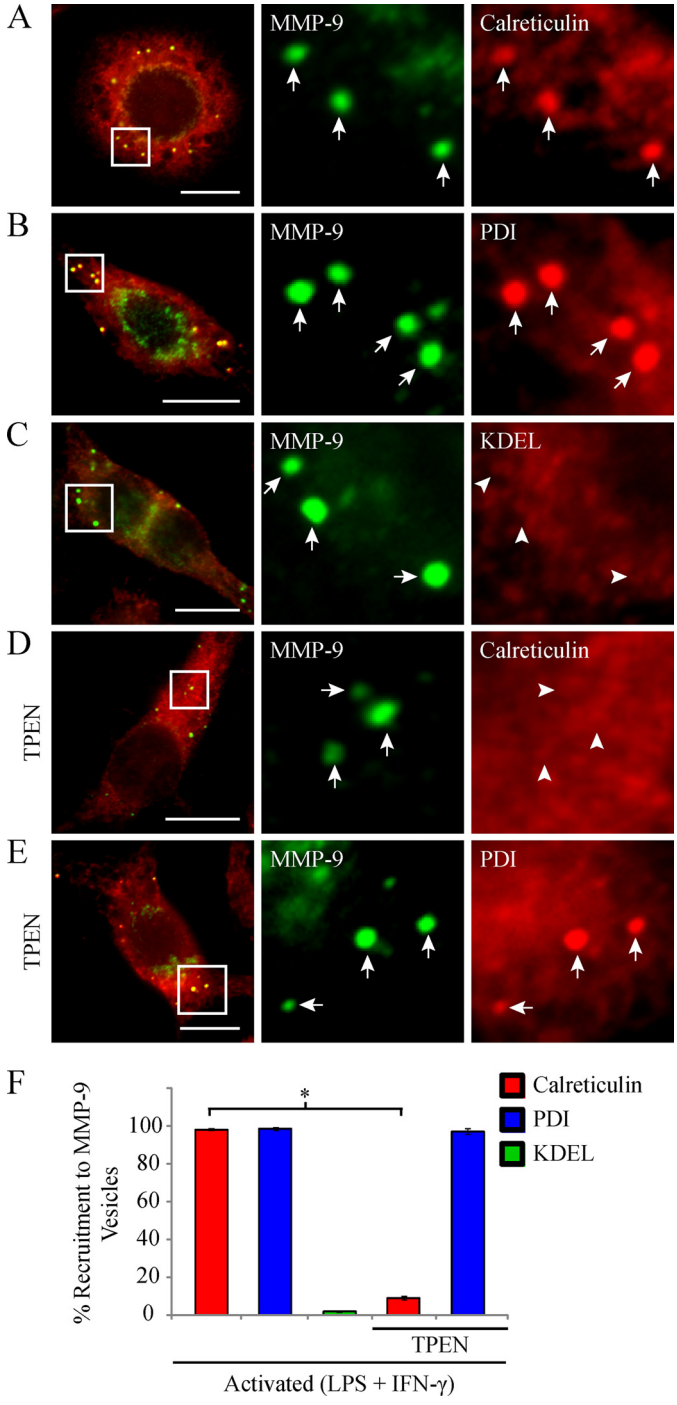

FIGURE 4. **Macrophage MMP-9 vesicles colocalize with the ER markers calreticulin and PDI but not KDEL.** RAW 264.7 cells were activated (0.1 μg/ml LPS and 100 units/ml IFN-γ for 9 h) and fixed and immunostained for MMP-9 (*green*) and calreticulin (*A*), PDI (*B*), or KDEL (*C*) (*red*). As well, some RAW 264.7 cells were treated with 1.5 μM TPEN, a zinc-chelating agent, during activation and were analyzed for MMP-9 (*green*) and calreticulin (*D*) or PDI (*E*) (*red*). The *arrows* indicate colocalization between MMP-9 vesicles and the indicated marker, whereas the *arrowheads* indicate the absence of co-recruitment. Note that images displayed are of cells containing higher than usual numbers of MMP-9 vesicles to sufficiently demonstrate a representative degree of colocalization with the indicated marker and may not be representative of the average number of MMP-9 vesicles per activated macrophage. *Scale bars*, 10 μm. The percentage of MMP-9 vesicles showing co-recruitment with the indicated markers was quantified (*F*). *, $p < 0.05$. *Error bars*, S.E.

Calreticulin has been shown to directly associate with PDI in a zinc-dependent manner (47). We therefore tested whether the zinc ion found in the catalytic domain of MMP-9 (2) may provide a structural necessity for the recruitment of calreticulin and PDI to MMP-9 vesicles. To test this, macrophage cells were treated with a zinc-chelating agent, TPEN, upon classical activation. Epifluorescent imaging of TPEN-treated cells revealed a striking absence of calreticulin from MMP-9 vesicles (Fig. 4*D*). Only 9.3 ± 0.9% of MMP-9 vesicles were calreticulin-positive in TPEN-treated cells, significantly lower than that observed in untreated cells (Fig. 4*F*). Interestingly, PDI recruitment to MMP-9 vesicles was unaffected by TPEN treatment (Fig. 4*E*). Similar to untreated cells, TPEN-treated cells showed 97.3 ± 0.5% of MMP-9 vesicles positive for PDI (Fig. 4*F*).

To determine if macrophage activation was inducing an ER stress response, we next investigated whether the MMP-9 punctate structures were vesicles of proteins targeted for intracellular degradation. Mammalian cells degrade cytoplasmic proteins and organelles mainly through the ubiquitin-proteosome or the autophagy-lysosome systems (48). The ubiquitin-proteosome pathway is typically responsible for the degradation of cytosolic proteins with short half-lives (49). It is also involved in ER quality control, in which misfolded proteins are translocated to the cytosol, where they are ubiquitinylated and targeted for degradation by proteosomes (48). To test for this kind of degradation, we immunostained activated RAW 264.7 cells for ubiquitinylated proteins and MMP-9 (Fig. 5*A*). We found by epifluorescent imaging that the MMP-9 vesicles were generally not marked by ubiquitinylation, with only 1.2 ± 0.4% of vesicles being positive (Fig. 5*D*). Therefore, MMP-9 vesicles were probably not targeted for degradation by proteosomes. The autophagy-lysosome pathway is typically responsible for clearing of cytosolic proteins with relatively long half-lives (49). These proteins are enclosed within autophagosomes that fuse with lysosomes to form autophagolysosomes. Accordingly, the contents of the autophagolysosomes are degraded by the action of lysosomal acid hydrolases (48). To test for autophagic degradation, we expressed RFP-tagged light chain 3 (LC3), an autophagosome-specific protein, in activated RAW 264.7 cells and immunostained for MMP-9. Additionally, we immunostained activated RAW 264.7 cells for LAMP-1, a lysosome membrane protein, and MMP-9. Epifluorescent imaging of these cells revealed that MMP-9 vesicles did not contain RFP-LC3 (Fig. 5*B*) or LAMP-1 (Fig. 5*C*). Only 0.67 ± 0.3 and 2.3 ± 0.7% of MMP-9 vesicles were positive for LC3 and LAMP-1, respectively (Fig. 5*D*). Thus it appears that macrophage MMP-9-containing vesicles were not targeted for intracellular degradation.

Vesicular Trafficking and Secretion of MMP-9 Is Dependent on MT Cytoskeleton in Activated Macrophages—We observed that activated RAW 264.7 cells sort MMP-9 into calreticulin- and PDI-containing vesicles. We next wanted to investigate the intracellular means of MMP-9 vesicular trafficking and secretion in these cells. It has been well established that the cytoskeleton is involved in the trafficking of organelles and vesicles (50). An MT-dependent secretion for MMP-9 has been implicated in melanoma cells (51), astrocytes (52), and neurons (53). To investigate its potential role in the trafficking of MMP-9 vesicles in activated macrophages, we immunostained activated RAW 264.7 cells for α-tubulin and MMP-9. Imaging of the basal cell area by total internal reflection microscopy revealed MMP-9 vesicles near the cell surface in close association with the MT cytoskeleton (supplemental Fig. 1). Quantitative colocalization analysis between MMP-9 and α-tubulin yielded a Pearson's coefficient of 0.44 ± 0.03. To investigate the possibility and extent of accidental overlap, a similar analysis performed on images with MMP-9 rotated along the *y* axis relative to the MT images (not shown) revealed a significantly lower Pearson's coefficient of 0.08 ± 0.04. To test MT dependence for MMP-9 secretion, RAW 264.7 cells were activated for 6 h prior to an additional 3 h in the presence of 10 μM nocodazole or left activated or resting. Nocodazole is a pharmacological agent that binds to tubulin dimers and prevents assembly into MT polymers. At high concentrations, the result is a net depolymerization of MTs in the cell over a short time frame (54). Epifluo-

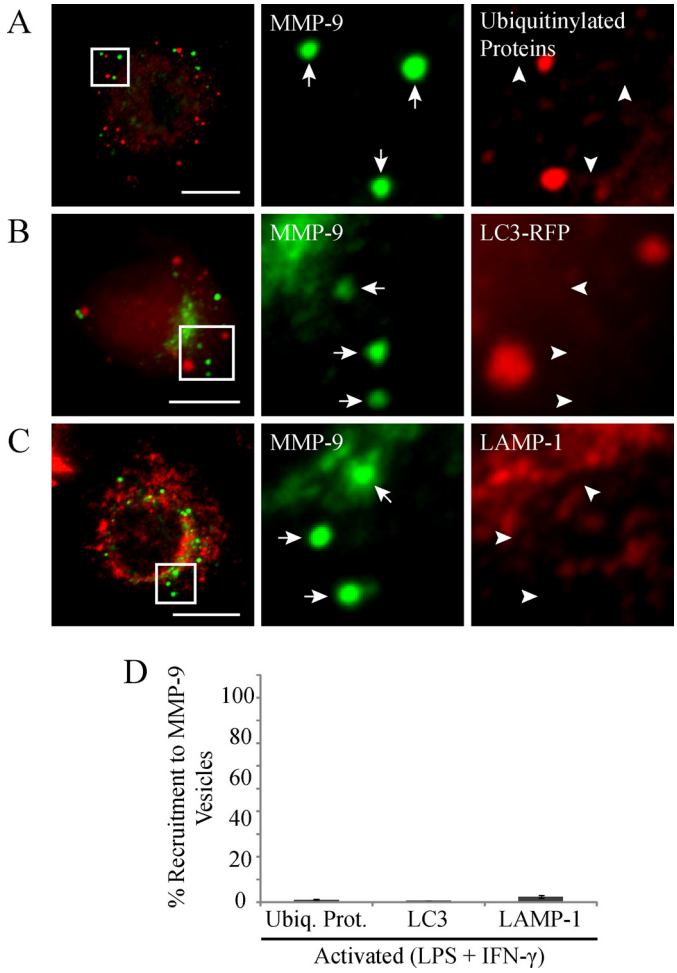

FIGURE 5. **MMP-9 vesicles do not colocalize with markers of proteosomal, lysosomal, or autophagic degradation.** Some RAW 264.7 cells were transfected with RFP-tagged LC3. Cells were stimulated with LPS/IFN-γ (0.1 μg/ml and 100 units/ml, respectively, for 9 h). Cells were fixed and immunostained for MMP-9 (*green*) and immunostained for ubiquitinylated proteins (*A*) or analyzed for LC3-RFP (*B*) or immunostained for LAMP-1 (*C*) (*red*) and examined by epifluorescent microscopy. The *arrows* identify MMP-9 vesicles, whereas the *arrowheads* indicate the absence of co-recruitment to MMP-9 vesicles. These cells had a robust amount of MMP-9 vesicles and represent the relative degrees of colocalization with the indicated markers. *Scale bars*, 10 μm. The percentage of MMP-9 vesicles showing co-recruitment with the indicated markers was quantified (*D*). *Error bars*, S.E.

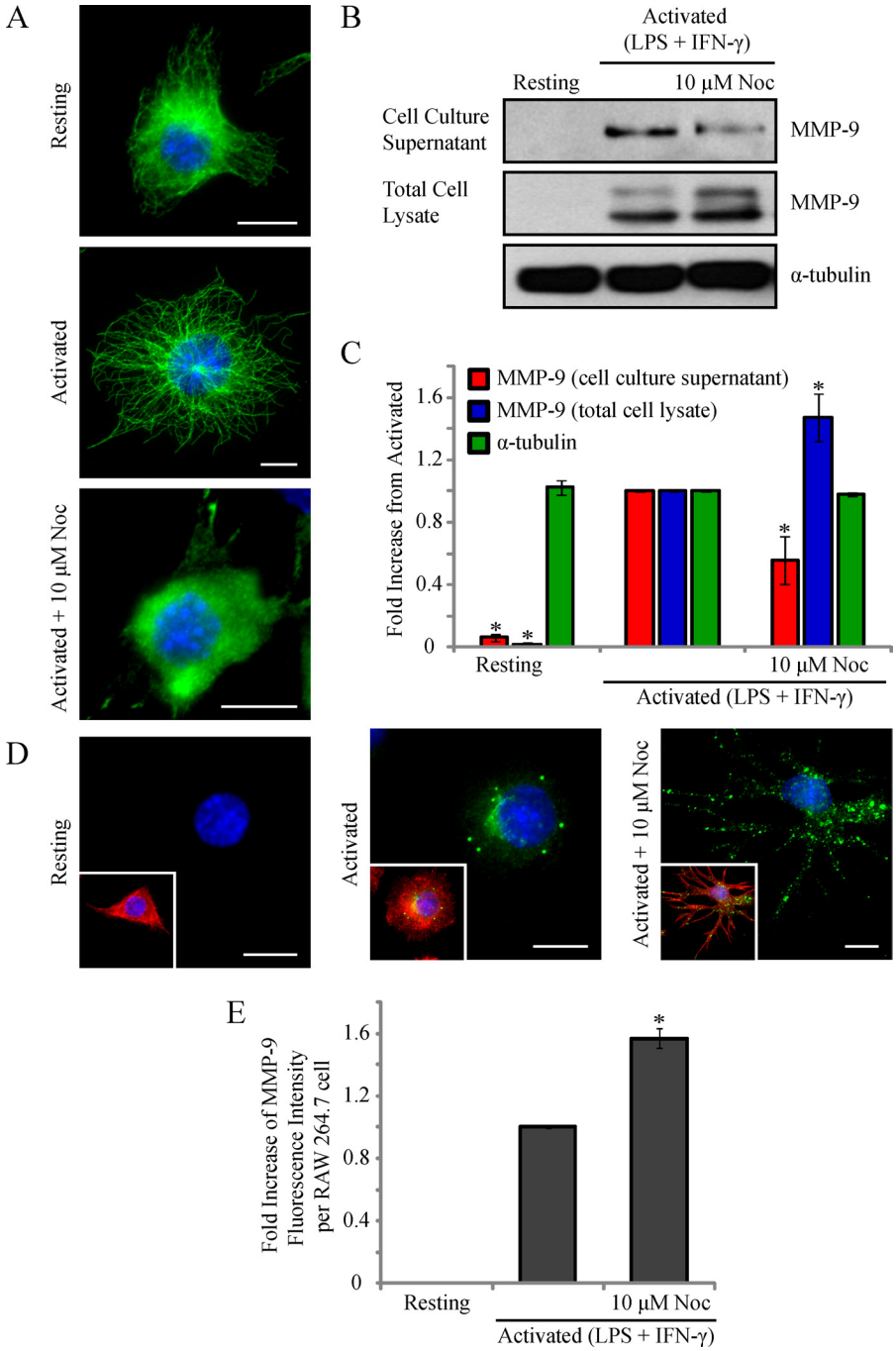

FIGURE 6. **Disruption of the MT cytoskeleton reduces MMP-9 secretion in activated macrophages.** RAW 264.7 cells were activated (0.1 μg/ml LPS and 100 units/ml IFN-γ for 9 h) in the presence of 10 μM nocodazole for 3 h. Cells were fixed and immunostained for α-tubulin (*green*) and DAPI (*blue*). *Scale bars*, 10 μm (*A*). Alternatively, the cell culture supernatants were collected, and the cells were lysed, and the supernatants and lysates were subjected to Western blotting (*B*) and densitometric analysis (*C*) for MMP-9 and α-tubulin. *, $p < 0.05$ compared with activated cells. Additionally, cells were fixed and analyzed for MMP-9 (*green*), phalloidin (*red*), and DAPI (*blue*) (*D*). *Scale bars*, 10 μm. The total fluorescence intensity of MMP-9 was measured using ImageJ software (*E*). *, $p < 0.05$ compared with activated cells. *Error bars*, S.E.

rescent imaging of α-tubulin revealed an efficient disruption of the MT cytoskeleton in activated cells treated with nocodazole compared with activated or resting macrophages (Fig. 6*A*). The cell culture supernatants and total cell lysates of RAW 264.7 cells were collected and subjected to Western blotting (Fig. 6*B*) and densitometric analysis (Fig. 6*C*). Compared with activated cells, nocodazole-treated cells showed a statistically significant reduction of MMP-9 in the cell culture supernatant. Concurrently, these cells showed a significant increase in intracellular MMP-9 levels. In addition to serving as a loading control, the unchanged levels of α-tubulin confirmed that the disruption of MMP-9 secretion was a result of nocodazole-induced MT disorganization rather than a reduction of subunit levels. Activated cells treated with nocodazole demonstrated an accumulation of MMP-9 vesicles intracellularly by epifluorescence (Fig. 6*D*) and a statistically significant increase in MMP-9 fluorescence intensity (Fig. 6*E*) compared with activated cells alone. Disruption of the MT cytoskeleton, such as that caused by

nocodazole treatment, causes dispersal of the Golgi apparatus into fragments throughout the cell (55). To verify that the observed accumulated vesicles were not solely MMP-9-containing Golgi fragments, we immunostained activated cells treated with nocodazole for GM130 and MMP-9 (supplemental Fig. 2). These cells showed some Golgi fragments positive for MMP-9 but also an accumulation of other MMP-9 vesicles that were not Golgi-positive. Collectively, these results indicate that an intact MT cytoskeleton is necessary for the trafficking of MMP-9 vesicles to the cell exterior.

Enhanced MT Stabilization Observed after Macrophage Activation Mediates Efficient Targeting of MMP-9 to Extracellular Space—We reported previously that classical activation of macrophages results in enhanced levels of stable cytoplasmic MTs and showed that this stabilization was important for increased cell spreading and phagocytic capabilities (9, 56). We next monitored the level of MT stabilization in RAW 264.7 cells activated (0.1 μg/ml LPS and 100 units/ml IFN-γ) for 9 h, using an anti-acetylated tubulin antibody (16). Epifluorescent imaging of RAW 264.7 cells immunostained for acetylated α-tubulin and α-tubulin revealed a marked increase in the degree of MT acetylation, occurring in patches along individual MT strands, in activated cells compared with resting cells (Fig. 7*A*). A significant increase in acetylated MT levels after activation was verified by immunoblotting for acetylated α-tubulin (Fig. 7, *B* and *C*).

We next wanted to determine whether the enhanced MT stabilization observed in activated macrophages was important for MMP-9 trafficking and secretion to the cell exterior. To begin, we investigated whether MMP-9 vesicles were adjacent to stable cytoplasmic MTs. To visualize the subpopulation of stable MTs, activated RAW 264.7 cells were immunostained for acetylated α-tubulin or MAP4 (9), total α-tubulin, and MMP-9. Epifluorescent imaging showed that 61.3 $\pm$ 3.7 or 66.7 $\pm$ 2.4% of MMP-9 vesicles were found along MTs post-translationally modified with acetylation (Fig. 7, *D* and *F*) or bound to MAP4 (Fig. 7, *E* and *F*), respectively, indicating that these vesicles probably associate with stabilized MTs for trafficking. To investigate this, we sought to determine if MT stabilization in activated macrophages played a functional role for MMP-9 secretion. We examined the effects of further exaggerating MT stabilization on the extent of MMP-9 secretion in activated macrophages. To increase MT stabilization, taxol, a drug that enhances the rate and yield of MT assembly (57), was used. RAW 264.7 cells were activated for 8 h and incubated for another 1 h in the presence of taxol at 0.1 μM or left activated or resting. Epifluorescent imaging of RAW 264.7 cells revealed completely stabilized MTs in activated/taxol-treated cells, indicated by acetylation along the entire lengths of MTs compared with the patches of acetylation observed in activated cells (Fig. 8*A*). The cell culture supernatants and total cell lysates of these cells were analyzed by Western blotting. Compared with activated cells, the cell culture supernatants of activated/taxol-treated cells showed increased MMP-9 levels, whereas the total cell lysates demonstrated reduced MMP-9 levels and enhanced acetylated α-tubulin levels (Fig. 8*B*). Following densitometric analysis, we observed a statistically significant increase in extracellular MMP-9 levels in activated cells treated with taxol com-

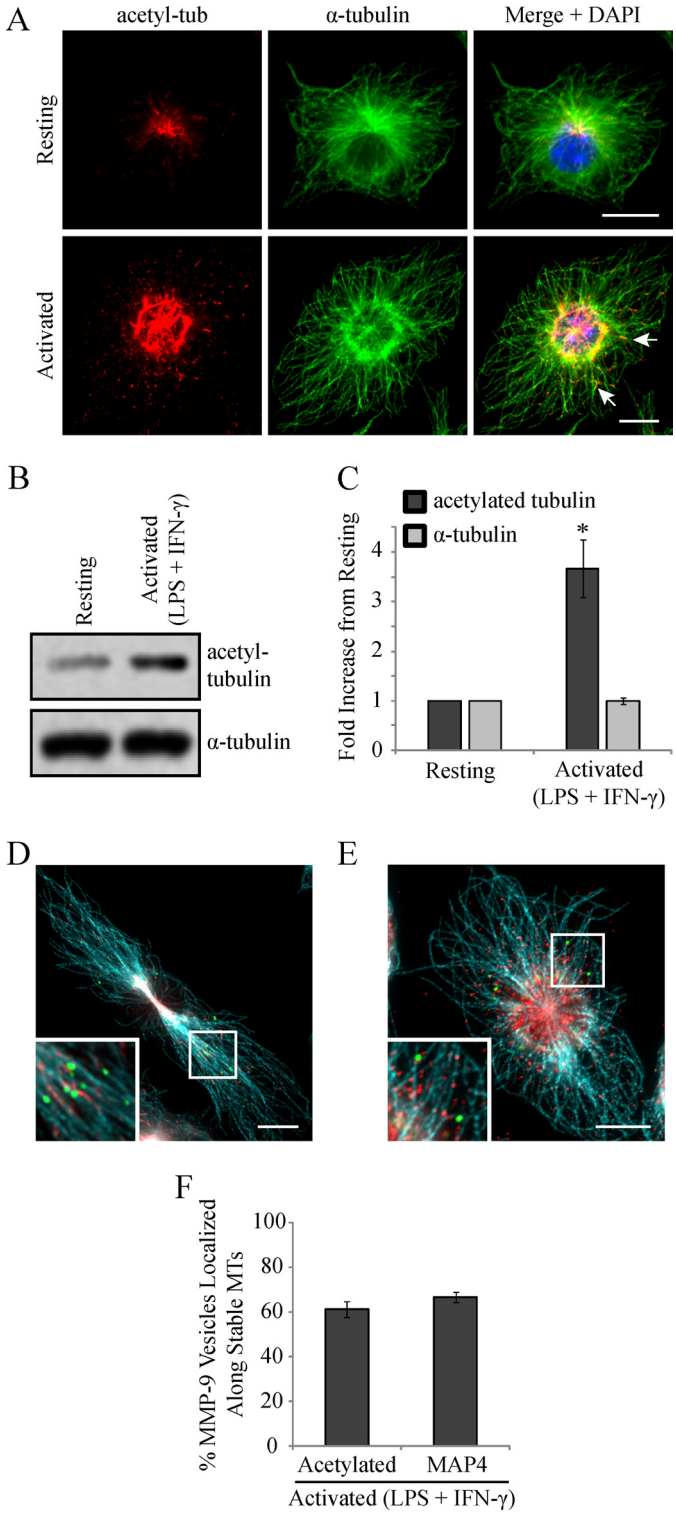

FIGURE 7. **MMP-9 vesicles localize along a subpopulation of stable MTs, exhibited after macrophage activation.** RAW 264.7 cells were activated (0.1 μg/ml LPS and 100 units/ml IFN-γ for 9 h), fixed, and immunostained for acetylated tubulin and α-tubulin and imaged by epifluorescence (*A*). The *arrows* indicate patches of acetylation occurring along the length of MT strands. Alternatively, the cells were lysed, and lysates were subjected to Western blotting (*B*) and densitometric analysis (*C*). *, $p < 0.05$ compared with activated cells. Fixed cells were also immunostained for MMP-9 (*green*), α-tubulin (*blue*), and acetylated α-tubulin (*D*) or MAP4 (*E*) (*red*). *Insets* show a higher magnification of MMP-9 vesicles and the MT cytoskeleton. *Scale bars*, 10 μm. The percentage of MMP-9 vesicles that localized along stabilized MTs was quantified (*F*). *Error bars*, S.E.

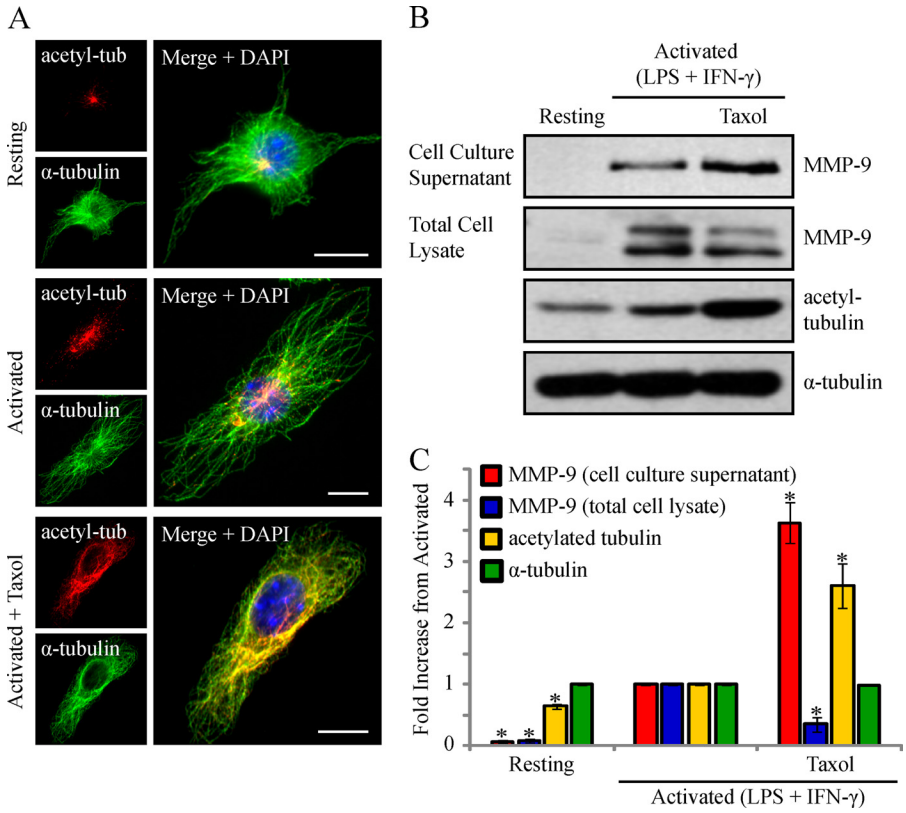

FIGURE 8. **Activated macrophages treated with taxol to enhance MT stabilization show increased levels of MMP-9 secretion.** RAW 264.7 cells were activated (0.1 μg/ml LPS and 100 units/ml IFN-γ for 9 h) and treated with 0.1 μM taxol for 1 h. Cells were fixed and immunostained for acetylated α-tubulin (*red*), α-tubulin (*green*), and DAPI (*blue*) (*A*). *Scale bars*, 10 μm. Alternatively, the cell culture supernatants were collected, the cells were lysed, and the supernatants and lysates were subjected to Western blotting (*B*) and densitometric analysis (*C*) for MMP-9, acetylated tubulin, and α-tubulin. *, $p < 0.05$ compared with activated cells. *Error bars*, S.E.

pared with activated cells alone (Fig. 8*C*). We also observed a statistically significant decrease in intracellular MMP-9 levels that corresponded to a significant increase in acetylated α-tubulin in activated/taxol-treated cells compared with activated cells alone (Fig. 8*C*). Taxol has been shown to stabilize MTs by binding directly to individual polymers (57) as well as by activating TLR4 in a similar way as LPS (58). Although resting RAW 264.7 cells treated with taxol did not show any intracellular or extracellular MMP-9 by Western blotting (data not shown), we wanted to verify that the enhanced secretion was a result of enhanced MT stabilization and not a synergistic effect of LPS and taxol ligation on TLR4. Therefore, we used an alternative way to enhance MT stabilization, by treating cells with a low dose of nocodazole (59).

Although nocodazole is typically used to depolymerize MTs, *in vitro* studies have shown that using nanomolar concentrations of nocodazole actually increases MT stabilization by suppressing MT dynamic instability and increasing the time MTs spend in a paused state (54, 59). Immunofluorescent imaging of RAW 264.7 cells activated for 6 h prior to an additional 3 h in the presence of 0.1 μM nocodazole revealed a less elaborate but fully stabilized MT network compared with activated cells (Fig. 9*A*). The cell culture supernatants and total cell lysates of these cells were analyzed by Western blotting. Compared with activated cells, the cell culture supernatants of activated cells treated with low dose nocodazole showed increased MMP-9 levels, whereas the total cell lysates possessed reduced MMP-9 levels and enhanced acetylated tubulin levels (Fig. 9*B*). Following densitometric analysis, we observed a statistically significant increase in extracellular MMP-9 levels in activated cells treated with low dose nocodazole compared with activated cells alone (Fig. 9*C*). We also observed a statistically significant decrease in the intracellular levels of MMP-9, with an expected enhancement of acetylated α-tubulin, in activated cells treated with low dose nocodazole compared with activated cells alone (Fig. 9*C*). Collectively, these data indicated that MT stabilization was a critical element of macrophage activation to efficiently drive newly synthesized MMP-9 vesicles to the extracellular space.

KIF5B and KIF3B Kinesin Isoforms Mediate MMP-9 Trafficking in Activated Macrophages—We have previously demonstrated, in a large scale proteomic analysis of MT-associated proteins, that association of the kinesin KIF5B isoform with MTs is significantly increased after macrophage classical activation (9). To bolster this finding, we performed a co-immunoprecipitation assay to pull down kinesin 5B and look for association with tubulin. Triggered by LPS/IFN-γ, we observed an enhanced association of kinesin with tubulin in activated macrophages compared with resting macrophages (Fig. 10, *A* and *B*). Recently, we have shown that kinesin 5B is the major MT motor involved in vesicle targeting to active plasma membrane regions during the process of phagocytosis in macrophages (60). Having demonstrated a functional role for MTs in MMP-9 trafficking and an enhanced association of kinesin 5B

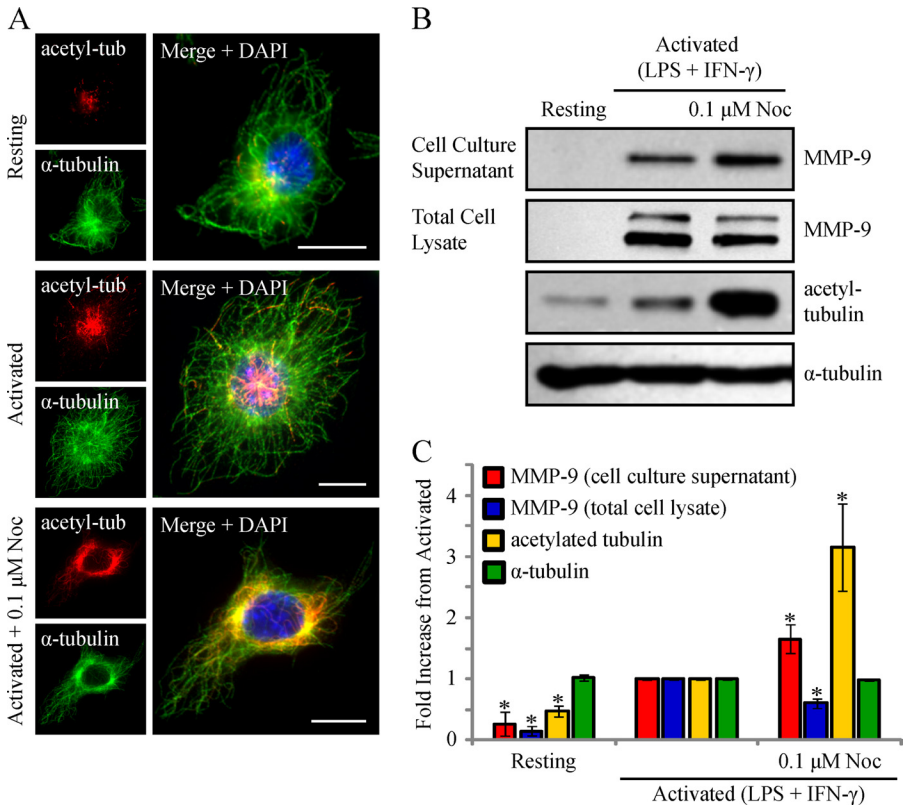

FIGURE 9. **Activated macrophages treated with low dose nocodazole (*Noc*) to enhance MT stabilization show increased levels of MMP-9 secretion.** RAW 264.7 cells were activated (0.1 μg/ml LPS and 100 units/ml IFN-γ for 9 h) and treated with 0.1 μM nocodazole for 3 h. Cells were fixed and immunostained for acetylated α-tubulin (*red*), α-tubulin (*green*), and DAPI (*blue*) (*A*). *Scale bars*, 10 μm. Alternatively, the cell culture supernatants were collected, the cells were lysed, and the supernatants and cell lysates were subjected to immunoblotting (*B*) and densitometric analysis (*C*) for MMP-9, acetylated α-tubulin, and α-tubulin. *, $p < 0.05$ compared with activated cells. *Error bars*, S.E.

with MTs in activated macrophages, we next wanted to see if kinesin 5B associated with MMP-9 vesicles. Confocal imaging of activated RAW 264.7 cells immunostained for MMP-9 and kinesin using a KIF5B-specific antibody revealed that MMP-9 vesicles colocalized with kinesin 5B (Fig. 10*C*). Quantitative colocalization analysis between MMP-9 and KIF5B yielded a Pearson's coefficient of 0.42 ± 0.03. To investigate the possibility of accidental overlap, a similar analysis performed on images with MMP-9 images rotated along the *y* axis relative to the KIF5B images (not shown) revealed a significantly lower Pearson's coefficient of 0.1 ± 0.02. We next investigated the potential role of the biosynthetic Rabs, Rab3D and Rab27b, in mediating the association of MMP-9 vesicles with kinesin. To do this, we expressed dominant negative versions of either Rab3D or Rab27b and assessed the extent of kinesin association with MMP-9 vesicles compared with untransfected cells. Cells expressing GFP-tagged Rab3D-DN revealed MMP-9 vesicles that no longer colocalized with kinesin 5B (Fig. 10*D*) and demonstrated a statistically lower Pearson's coefficient of 0.04 ± 0.02 compared with 0.42 ± 0.03 in untransfected cells (Fig. 10*C*). However, kinesin-MMP-9 association in cells expressing GFP-tagged Rab27b-DN was unaffected (Fig. 10*E*) and revealed a Pearson's coefficient of 0.49 ± 0.03, similar to that seen in untransfected cells. Overall, these data demonstrated an enhanced recruitment of kinesin 5B to MTs after macrophage activation, which depends on Rab3D for association with MMP-9 vesicles.

We next examined the effects of KIF5B inhibition in activated macrophages by expressing a KIF5B rigor mutant (61), which demonstrated an altered cellular distribution (Fig. 11*B*) compared with WT KIF5B (Fig. 10*C*). Kinesin rigor mutants have been shown to tightly bind to MTs due to a mutation in the ATP-binding domain preventing their dissociation (61, 62). Therefore, the observed change in KIF5B cellular distribution of the rigor mutant is probably due to its tight attachment to MTs compared with WT KIF5B. Cells expressing the KIF5B rigor mutant demonstrated a pronounced accumulation of intracellular MMP-9 vesicles (Fig. 11, *B* and *D*) compared with untransfected cells (Fig. 11, *A* and *D*). Recently, it has been shown that MT1-MMP secretion is regulated by more than one kinesin isoform (61). We therefore investigated the effects of expressing a KIF3B rigor mutant (61) on MMP-9 accumulation. Activated macrophages expressing the KIF3B rigor mutant revealed a similar accumulation of MMP-9 vesicles as cells expressing the KIF5B rigor mutant (Fig. 11, *C* and *D*), showing a significant increase in the average number of MMP-9 vesicles per cell compared with untransfected cells (Fig. 11*D*). Disrupting retrograde transport via dynein by overexpression of GFP-tagged dynamitin p50 had no impact on MMP vesicle production and distribution in activated macrophages (data not shown). Thus, MMP-9 secretion was Rab3D-dependent and relied on both KIF5B and KIF3B kinesin isoforms.

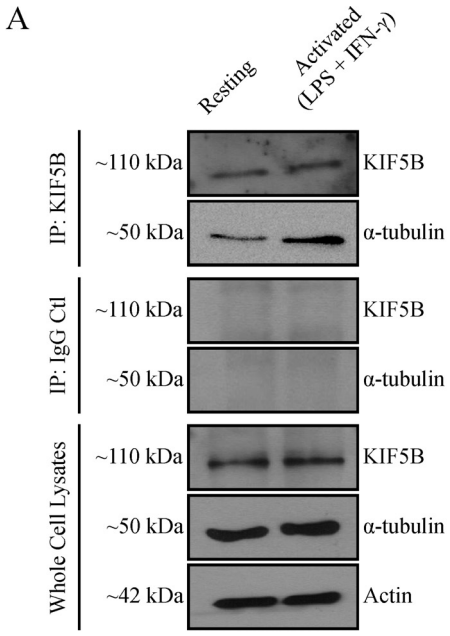

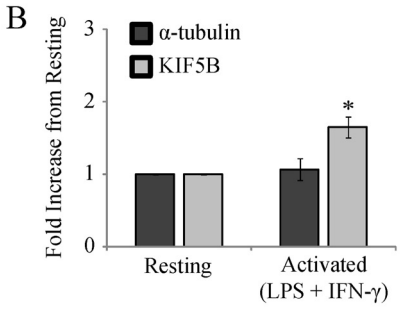

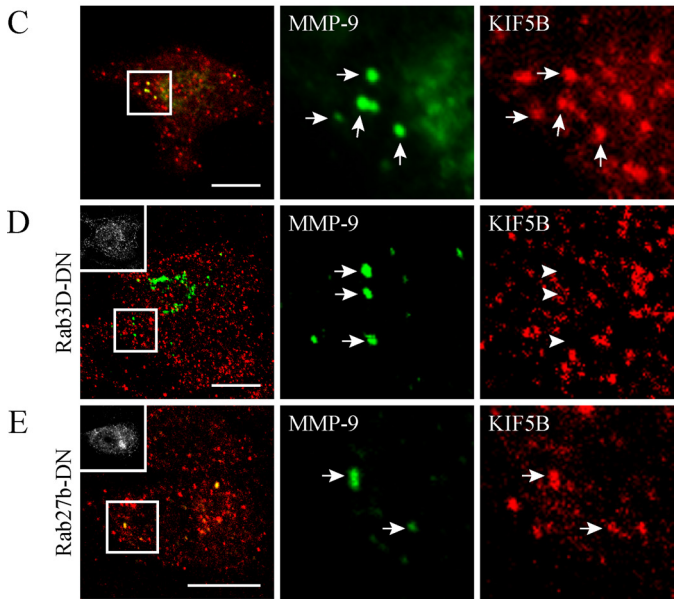

FIGURE 10. **MMP-9 vesicles associate with the MT motor kinesin 5B in a Rab3D-dependent manner.** RAW 264.7 cells were activated (0.1 μg/ml LPS and 100 units/ml IFN-γ for 9 h) or left resting. Cell lysates were processed for immunoprecipitation using either kinesin 5B antibody (*A*, *top*) or IgG control antibody (*A*, *middle*) and analyzed by Western blotting for KIF5B and α-tubulin. As well, some cell lysate was processed directly for Western blotting and analyzed for KIF5B, α-tubulin, and actin (*A*, *bottom*). Densitometric analysis was performed on KIF5B and α-tubulin resulting from immunoprecipitation with a KIF5B antibody (*B*). *, $p < 0.05$ compared with resting cells. Alternatively, activated cells untransfected (*C*) or expressing Rab3D-DN-GFP (*D*) or Rab27b-DN-GFP (*E*) were fixed and immunostained for MMP-9 (*green*) and kinesin 5B (*red*). *Insets* show transfected cells. *Scale bars*, 10 μm. The *arrows* indicate colocalization with kinesin 5B, whereas the *arrowheads* indicate a lack of colocalization. *Error bars*, S.E.

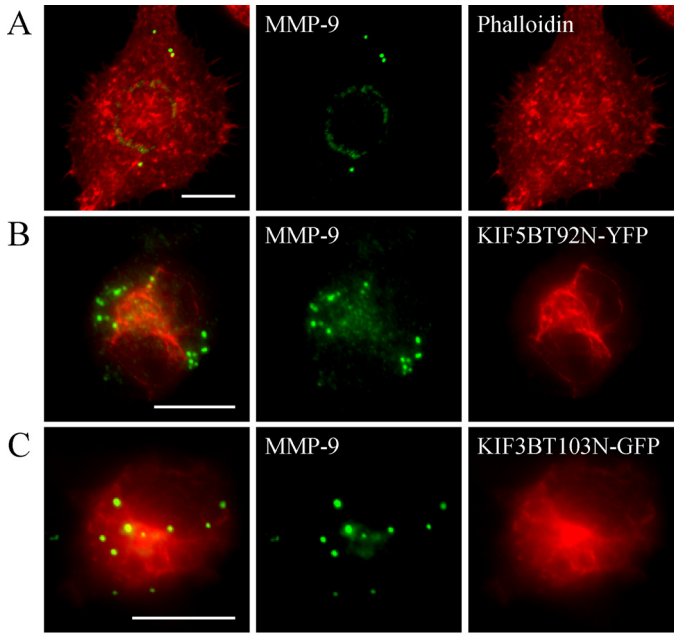

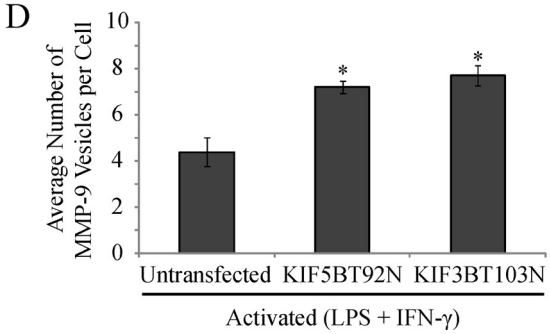

FIGURE 11. **Trafficking of MMP-9 vesicles is mediated by the MT motors kinesin 5B and 3B in activated macrophages.** Activated (0.1 μg/ml LPS and 100 units/ml IFN-γ for 9 h) RAW 264.7 cells either untransfected or expressing kinesin 5B or 3B rigor mutants were fixed and immunostained for MMP-9 (*green*). Untransfected cells were stained with phalloidin to mark the cell periphery (*A*) (*red*). Alternatively, transfected cells were analyzed for either KIF5BT92N-YFP (*B*) or KIF3BT103N-GFP (*C*) (*red*). *Scale bars*, 10 μm. A quantification of the average number of MMP-9 vesicles per macrophage cell was performed (*D*). *, $p < 0.05$ compared with resting cells. *Error bars*, S.E.

DISCUSSION

The primary goal of this work was to characterize the distribution of MMP-9 in activated macrophages and to elucidate the mechanism by which it is trafficked and secreted. A summary of the composition of MMP-9 vesicles as well as their trafficking along stable MTs in activated macrophages is depicted in Fig. 12.

MMP-9 is a heavily glycosylated glycoprotein, where 15% of its mass is contributed by post-translational glycosylation (63). Although the function of such glycosylation has not been investigated for MMP-9, it has been suggested to regulate substrate targeting for membrane type 1-MMP (64). We have demonstrated for the first time an intermediate 89-kDa form of

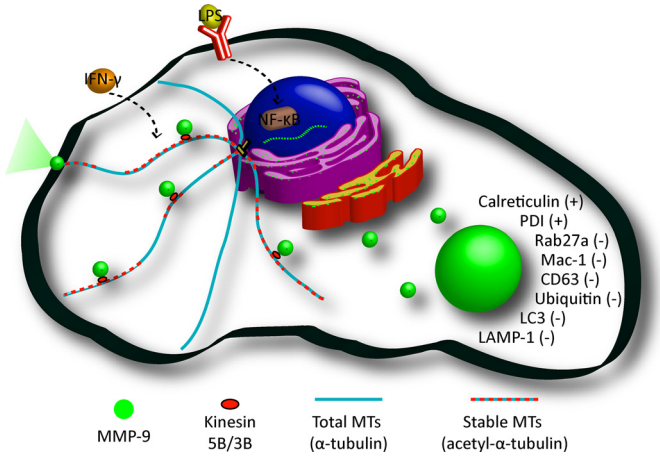

FIGURE 12. **A model of MMP-9 sorting and trafficking in activated macrophages.** Activated macrophages exhibit increased levels of stable cytoplasmic MTs with increased production and trafficking of MMP-9. MMP-9 is processed through the biosynthetic pathway and is sorted in discrete vesicular organelles that contain calreticulin and PDI and do not colocalize with markers of neutrophil tertiary granules or intracellular degradation. Shown are MMP-9 vesicles being trafficked along stabilized MTs by the molecular motors kinesin 5B and 3B.

MMP-9 that appears in activated cells treated with BFA by immunoblotting. BFA inhibits ER to Golgi transport (35), and we demonstrated that activated cells treated with BFA show MMP-9 localized to the ER by immunofluorescence. Therefore, we can attribute any glycosylation of the 85-kDa form of MMP-9 in these BFA-treated cells to the ER. This provides insight into the glycosylation patterns that MMP-9 undergoes through the biosynthetic pathway, whereby the ER is responsible for maturing MMP-9 from its 85-kDa underglycosylated form to its 89-kDa intermediate glycosylated form. Additionally, we can infer that full glycosylation of the 89-kDa form to the 92-kDa form occurs in the Golgi apparatus. In activated cells not treated with BFA, we observe substantial amounts of the 85- and 92-kDa forms and do not detect the 89-kDa intermediate. This may suggest that the 85-kDa form is rapidly processed, and the 89-kDa form is a transient intermediate.

Although MMP-9 originates from the same gene in neutrophils and in peripheral blood monocytes (63), we showed by epifluorescence that macrophages package MMP-9 into vesicles that differ in composition from neutrophil gelatinase granules. Neutrophils make up the first wave of leukocytes to arrive at the site of inflammation and, as such, need to be able to migrate without hesitation (31). Unlike macrophages, neutrophils produce and prepack MMP-9 in tertiary granules to allow for rapid release upon stimulation, without the need for transcription and translation (31). Therefore, release of neutrophil MMP-9 probably relies on post-translational control of vesicle trafficking, whereas release of macrophage MMP-9 relies on transcriptional induction and subsequent secretion. We speculate that macrophage MMP-9 vesicles do not require regulation by Rab27a because the vesicles are produced only when the macrophage is immunologically challenged. Neutrophils do not produce TIMP-1 and, as a result, are unable to control MMP-9 activity by forming MMP-9·TIMP-1 complexes (63). Conversely, macrophages have been shown to produce TIMP-1 and are able to form these complexes (2). Packaging of the adhesion molecule Mac-1 with MMP-9 in neutrophils may thus ensure that MMP-9 will only be released at sites of firm attachment with endothelial components (37), a control measure probably needed by neutrophils because they cannot provide control by TIMPs.

Having demonstrated a compositional difference between neutrophil and macrophage MMP-9-containing vesicles, we next investigated their identity in macrophages. We showed that the normally ER-resident proteins, calreticulin and PDI, are sorted with MMP-9 in discrete vesicles. Our observations showing that these vesicles were not positive for markers of proteosomal, lysosomal, and autophagic processing suggest that they are probably not targeted for intracellular degradation. ER-resident proteins are targeted and retained in the ER via a KDEL signal sequence. KDEL proteins that make their way to the Golgi apparatus are recognized by KDEL receptors and are transported back to the ER (44, 45). We did not observe KDEL staining localized to MMP-9 vesicular organelles in activated macrophages, which confirmed that these punctate structures were not expanded pockets within the ER; nor were they anterograde ER-to-Golgi vesicles or retrograde Golgi-to-ER vesicles. There is growing evidence that some ER proteins, such as calreticulin (65) and PDI (43), can be detected and function in non-ER locations. The exact means by which these proteins may evade the ER retention machinery is not well understood; however, some theories have been proposed. KDEL proteins may escape the ER in situations where KDEL receptors become saturated or in cases where ER proteins form complexes with other macromolecules or possibly when their KDEL signal sequence is removed (43, 66). Our observation that MMP-9 vesicles were devoid of KDEL staining implies that the calreticulin and PDI may have escaped ER retention by loss of their KDEL retention signals.

Calreticulin has been shown to associate directly with PDI in a zinc-dependent manner (47). We observed a zinc-dependent recruitment of calreticulin, and not PDI, to MMP-9 vesicles, suggesting that the zinc ion found in the catalytic domain of MMP-9 (2) may be a structural ingredient necessary for calreticulin recruitment. As well, these data suggest that PDI is recruited independently of calreticulin to MMP-9 vesicles. Because PDI is a chaperone responsible for forming disulfide bonds between the thiols of cysteine residues (67), we speculate that its association with MMP-9 occurs during MMP-9 formation, after which calreticulin recruitment is mediated via zinc availability in the MMP-9 catalytic domain.

Calreticulin has been described in non-ER compartments, such as the acrosomal vesicles of sperm cells and the cytotoxic granules of T-cells (65). In T-cell granules, calreticulin associates with perforin, which becomes activated in the presence of calcium. As a calcium-binding protein, calreticulin was proposed to regulate the levels of free calcium in these granules (65). Calcium also modulates MMP-9 stability (68), so the presence of calreticulin in MMP-9 vesicles of activated macrophages may maintain favorable calcium levels important for MMP-9 stability.

Stabilization of the MT cytoskeleton is uniquely rapid and predominant in activated macrophages, whereas other animal cells have largely dynamic MTs (13). We have previously dem-

onstrated that macrophage activation results in enhanced levels of stable cytoplasmic MTs (4, 9) as well as an enhanced association of the MT motor kinesin with MTs (9). More recently, we have implicated kinesin 5B in mediating vesicle targeting to active plasma membrane regions during the process of phagocytosis in macrophages (60). In the present study, we verified the enhanced MT stabilization and association of kinesin with MTs after macrophage activation and assessed their involvement in mediating the extensive trafficking of newly produced MMP-9 vesicles, required for macrophage migration (23, 28–30). We have demonstrated a MT-dependent secretion for MMP-9 and, using pharmacological agents to exaggerate MT stabilization, showed that enhanced MT stabilization further accelerates MMP-9 secretion. Additionally, we have implicated the MT motors kinesin 5B and 3B in mediating MMP-9 trafficking. We have shown that Rab3D, a known regulator of intracellular vesicle transport (69), plays a role in mediating the association of MMP-9 vesicles with kinesin. Acetylation of MTs is known to enhance the binding and motility of kinesin (70), and we speculate that enrichment of acetylated MTs after macrophage activation promotes enhanced kinesin binding on stable MT tracks that efficiently traffic MMP-9 to the cell exterior.

Despite its critical role in macrophage migration during the inflammatory response, excessive or unregulated production and secretion of MMP-9 results in its contribution to pathological processes (31). Excessive secretion of MMP-9 by macrophages was shown to cause extracellular matrix degradation that induces plaque rupture in the cephalic arteries of atherosclerosis mouse models (71). Additionally, patients with emphysema demonstrated alveolar macrophages as the most abundant inflammatory cell present in the lung, secreting elevated levels of MMP-9 compared with the cells of control patients (72). Our investigation of the mode by which MMP-9 is trafficked in activated macrophages may thus provide pertinent insight for the regulation of excessive MMP-9 secretion in disease states, such as atherosclerosis and emphysema.

Acknowledgments—DNA constructs were gifts obtained as follows. CD63-GFP was from Dr. Sergio Grinstein (The Hospital for Sick Children, Toronto, Canada); LC3-RFP was from Dr. Nicola Jones (The Hospital for Sick Children); KIF5BT92N-YFP and KIF3BT103N-GFP were from Stefan Linder (Universitätsklinikum Eppendorf, Hamburg, Germany). Goat polyclonal anti-calreticulin was a gift from Dr. Michal Opas (University of Toronto). We thank the Centre for the Neurobiology of Stress Facility (University of Toronto Scarborough) as well as the Cell Biology and Image Acquisition Core Facility (University of Ottawa) for access to advanced imaging systems.

REFERENCES

1. Ross, M. H., and Pawlina, W. (2006) *Histology: A Text and Atlas*, p. 256, Lippincott Williams and Wilkins, Baltimore
2. Webster, N. L., and Crowe, S. M. (2006) Matrix metalloproteinases, their production by monocytes and macrophages and their potential role in HIV-related diseases. *J. Leukoc. Biol.* **80,** 1052–1066
3. Mantovani, A., Sica, A., and Locati, M. (2007) New vistas on macrophage differentiation and activation. *Eur. J. Immunol.* **37,** 14–16
4. Binker, M. G., Zhao, D. Y., Pang, S. J., and Harrison, R. E. (2007) Cytoplasmic linker protein-170 enhances spreading and phagocytosis in activated macrophages by stabilizing microtubules. *J. Immunol.* **179,** 3780–3791
5. Wirth, J. J., Kierszenbaum, F., Sonnenfeld, G., and Zlotnik, A. (1985) Enhancing effects of γ interferon on phagocytic cell association with and killing of *Trypanosoma cruzi*. *Infect. Immun.* **49,** 61–66
6. Higginbotham, J. N., Lin, T. L., and Pruett, S. B. (1992) Effect of macrophage activation on killing of *Listeria monocytogenes*. Roles of reactive oxygen or nitrogen intermediates, rate of phagocytosis, and retention of bacteria in endosomes. *Clin. Exp. Immunol.* **88,** 492–498
7. Gordon, S. (2003) Alternative activation of macrophages. *Nat. Rev. Immunol.* **3,** 23–35
8. Khandani, A., Eng, E., Jongstra-Bilen, J., Schreiber, A. D., Douda, D., Samavarchi-Tehrani, P., and Harrison, R. E. (2007) Microtubules regulate PI-3K activity and recruitment to the phagocytic cup during Fcγ receptor-mediated phagocytosis in nonelicited macrophages. *J. Leukoc. Biol.* **82,** 417–428
9. Patel, P. C., Fisher, K. H., Yang, E. C., Deane, C. M., and Harrison, R. E. (2009) Proteomic analysis of microtubule-associated proteins during macrophage activation. *Mol. Cell Proteomics* **8,** 2500–2514
10. Nogales, E. (2000) Structural insights into microtubule function. *Annu. Rev. Biochem.* **69,** 277–302
11. Allen, L. A., and Aderem, A. (1996) Mechanisms of phagocytosis. *Curr. Opin Immunol.* **8,** 36–40
12. Billadeau, D. D., Nolz, J. C., and Gomez, T. S. (2007) Regulation of T-cell activation by the cytoskeleton. *Nat. Rev. Immunol.* **7,** 131–143
13. Desai, A., and Mitchison, T. J. (1997) Microtubule polymerization dynamics. *Annu. Rev. Cell Dev. Biol.* **13,** 83–117
14. Mitchison, T. J. (1995) Evolution of a dynamic cytoskeleton. *Philos. Trans. R. Soc. Lond. B Biol. Sci.* **349,** 299–304
15. Nguyen, H. L., Chari, S., Gruber, D., Lue, C. M., Chapin, S. J., and Bulinski, J. C. (1997) Overexpression of full- or partial-length MAP4 stabilizes microtubules and alters cell growth. *J. Cell Sci.* **110,** 281–294
16. Piperno, G., LeDizet, M., and Chang, X. J. (1987) Microtubules containing acetylated α-tubulin in mammalian cells in culture. *J. Cell Biol.* **104,** 289–302
17. Schulze, E., Asai, D. J., Bulinski, J. C., and Kirschner, M. (1987) Posttranslational modification and microtubule stability. *J. Cell Biol.* **105,** 2167–2177
18. Bulinski, J. C., and Gundersen, G. G. (1991) Stabilization of post-translational modification of microtubules during cellular morphogenesis. *BioEssays* **13,** 285–293
19. Min, D., Moore, A. G., Bain, M. A., Breit, S. N., and Lyons, J. G. (2002) Activation of macrophage promatrix metalloproteinase-9 by lipopolysaccharide-associated proteinases. *J. Immunol.* **168,** 2449–2455
20. Opdenakker, G., Van den Steen, P. E., and Van Damme, J. (2001) Gelatinase B. A tuner and amplifier of immune functions. *Trends Immunol.* **22,** 571–579
21. Rhee, J. W., Lee, K. W., Kim, D., Lee, Y., Jeon, O. H., Kwon, H. J., and Kim, D. S. (2007) NF-κB-dependent regulation of matrix metalloproteinase-9 gene expression by lipopolysaccharide in a macrophage cell line RAW 264.7. *J. Biochem. Mol. Biol.* **40,** 88–94
22. Fridman, R., Toth, M., Chvyrkova, I., Meroueh, S. O., and Mobashery, S. (2003) Cell surface association of matrix metalloproteinase-9 (gelatinase B). *Cancer Metastasis Rev.* **22,** 153–166
23. Gong, Y., Hart, E., Shchurin, A., and Hoover-Plow, J. (2008) Inflammatory macrophage migration requires MMP-9 activation by plasminogen in mice. *J. Clin. Invest.* **118,** 3012–3024
24. Ogata, Y., Enghild, J. J., and Nagase, H. (1992) Matrix metalloproteinase 3 (stromelysin) activates the precursor for the human matrix metalloproteinase 9. *J. Biol. Chem.* **267,** 3581–3584
25. von Bredow, D. C., Cress, A. E., Howard, E. W., Bowden, G. T., and Nagle, R. B. (1998) Activation of gelatinase-tissue-inhibitors-of-metalloproteinase complexes by matrilysin. *Biochem. J.* **331,** 965–972
26. Knäuper, V., Smith, B., López-Otin, C., and Murphy, G. (1997) Activation of progelatinase B (proMMP-9) by active collagenase-3 (MMP-13). *Eur. J. Biochem.* **248,** 369–373
27. Lambert, E., Dassé, E., Haye, B., and Petitfrère, E. (2004) TIMPs as multifacial proteins. *Crit. Rev. Oncol. Hematol.* **49,** 187–198
28. Pruijt, J. F., Fibbe, W. E., Laterveer, L., Pieters, R. A., Lindley, I. J., Paemen, L., Masure, S., Willemze, R., and Opdenakker, G. (1999) Prevention of

interleukin-8-induced mobilization of hematopoietic progenitor cells in rhesus monkeys by inhibitory antibodies against the metalloproteinase gelatinase B (MMP-9). *Proc. Natl. Acad. Sci. U.S.A.* **96,** 10863–10868
29. Watanabe, H., Nakanishi, I., Yamashita, K., Hayakawa, T., and Okada, Y. (1993) Matrix metalloproteinase-9 (92-kDa gelatinase/type IV collagenase) from U937 monoblastoid cells. Correlation with cellular invasion. *J. Cell Sci.* **104,** 991–999
30. Rahat, M. A., Marom, B., Bitterman, H., Weiss-Cerem, L., Kinarty, A., and Lahat, N. (2006) Hypoxia reduces the output of matrix metalloproteinase-9 (MMP-9) in monocytes by inhibiting its secretion and elevating membranal association. *J. Leukoc. Biol.* **79,** 706–718
31. Van den Steen, P. E., Dubois, B., Nelissen, I., Rudd, P. M., Dwek, R. A., and Opdenakker, G. (2002) Biochemistry and molecular biology of gelatinase B or matrix metalloproteinase-9 (MMP-9). *Crit. Rev. Biochem. Mol. Biol.* **37,** 375–536
32. Makowski, G. S., and Ramsby, M. L. (1996) Calibrating gelatin zymograms with human gelatinase standards. *Anal. Biochem.* **236,** 353–356
33. Olson, M. W., Bernardo, M. M., Pietila, M., Gervasi, D. C., Toth, M., Kotra, L. P., Massova, I., Mobashery, S., and Fridman, R. (2000) Characterization of the monomeric and dimeric forms of latent and active matrix metalloproteinase-9. Differential rates for activation by stromelysin 1. *J. Biol. Chem.* **275,** 2661–2668
34. Pfeffer, S. R., and Rothman, J. E. (1987) Biosynthetic protein transport and sorting by the endoplasmic reticulum and Golgi. *Annu. Rev. Biochem.* **56,** 829–852
35. Nebenführ, A., Ritzenthaler, C., and Robinson, D. G. (2002) Brefeldin A. Deciphering an enigmatic inhibitor of secretion. *Plant Physiol.* **130,** 1102–1108
36. Borregaard, N., and Cowland, J. B. (1997) Granules of the human neutrophilic polymorphonuclear leukocyte. *Blood* **89,** 3503–3521
37. Kjeldsen, L., Sengeløv, H., Lollike, K., Nielsen, M. H., and Borregaard, N. (1994) Isolation and characterization of gelatinase granules from human neutrophils. *Blood* **83,** 1640–1649
38. Brzezinska, A. A., Johnson, J. L., Munafo, D. B., Crozat, K., Beutler, B., Kiosses, W. B., Ellis, B. A., and Catz, S. D. (2008) The Rab27a effectors JFC1/Slp1 and Munc13–4 regulate exocytosis of neutrophil granules. *Traffic* **9,** 2151–2164
39. Skubitz, K. M., Campbell, K. D., and Skubitz, A. P. (2000) CD63 associates with CD11/CD18 in large detergent-resistant complexes after translocation to the cell surface in human neutrophils. *FEBS Lett.* **469,** 52–56
40. Rupani, R., Handerson, T., and Pawelek, J. (2004) Co-localization of β1,6-branched oligosaccharides and coarse melanin in macrophage-melanoma fusion hybrids and human melanoma cells *in vitro*. *Pigment Cell Res.* **17,** 281–288
41. Wu, M., Massaeli, H., Durston, M., and Mesaeli, N. (2007) Differential expression and activity of matrix metalloproteinase-2 and -9 in the calreticulin-deficient cells. *Matrix Biol.* **26,** 463–472
42. Opas, M., Dziak, E., Fliegel, L., and Michalak, M. (1991) Regulation of expression and intracellular distribution of calreticulin, a major calcium-binding protein of nonmuscle cells. *J. Cell. Physiol.* **149,** 160–171
43. Turano, C., Coppari, S., Altieri, F., and Ferraro, A. (2002) Proteins of the PDI family. Unpredicted non-ER locations and functions. *J. Cell. Physiol.* **193,** 154–163
44. Munro, S., and Pelham, H. R. (1987) A C-terminal signal prevents secretion of luminal ER proteins. *Cell* **48,** 899–907
45. Pelham, H. R. (1988) Evidence that luminal ER proteins are sorted from secreted proteins in a post-ER compartment. *EMBO J.* **7,** 913–918
46. Tang, B. L., Wong, S. H., Qi, X. L., Low, S. H., and Hong, W. (1993) Molecular cloning, characterization, subcellular localization and dynamics of p23, the mammalian KDEL receptor. *J. Cell Biol.* **120,** 325–338
47. Baksh, S., Burns, K., Andrin, C., and Michalak, M. (1995) Interaction of calreticulin with protein-disulfide isomerase. *J. Biol. Chem.* **270,** 31338–31344
48. Rubinsztein, D. C. (2006) The roles of intracellular protein degradation pathways in neurodegeneration. *Nature* **443,** 780–786
49. Cuervo, A. M., Stefanis, L., Fredenburg, R., Lansbury, P. T., and Sulzer, D. (2004) Impaired degradation of mutant α-synuclein by chaperone-mediated autophagy. *Science* **305,** 1292–1295
50. Goode, B. L., Drubin, D. G., and Barnes, G. (2000) Functional cooperation between the microtubule and actin cytoskeletons. *Curr. Opin Cell Biol.* **12,** 63–71
51. Schnaeker, E. M., Ossig, R., Ludwig, T., Dreier, R., Oberleithner, H., Wilhelmi, M., and Schneider, S. W. (2004) Microtubule-dependent matrix metalloproteinase-2/matrix metalloproteinase-9 exocytosis. Prerequisite in human melanoma cell invasion. *Cancer Res.* **64,** 8924–8931
52. Sbai, O., Ould-Yahoui, A., Ferhat, L., Gueye, Y., Bernard, A., Charrat, E., Mehanna, A., Risso, J. J., Chauvin, J. P., Fenouillet, E., Rivera, S., and Khrestchatisky, M. (2010) Differential vesicular distribution and trafficking of MMP-2, MMP-9, and their inhibitors in astrocytes. *Glia* **58,** 344–366
53. Sbai, O., Ferhat, L., Bernard, A., Gueye, Y., Ould-Yahoui, A., Thiolloy, S., Charrat, E., Charton, G., Tremblay, E., Risso, J. J., Chauvin, J. P., Arsanto, J. P., Rivera, S., and Khrestchatisky, M. (2008) Vesicular trafficking and secretion of matrix metalloproteinases-2, -9 and tissue inhibitor of metalloproteinases-1 in neuronal cells. *Mol. Cell Neurosci.* **39,** 549–568
54. Liao, G., Nagasaki, T., and Gundersen, G. G. (1995) Low concentrations of nocodazole interfere with fibroblast locomotion without significantly affecting microtubule level. Implications for the role of dynamic microtubules in cell locomotion. *J. Cell Sci.* **108,** 3473–3483
55. Cole, N. B., Sciaky, N., Marotta, A., Song, J., and Lippincott-Schwartz, J. (1996) Golgi dispersal during microtubule disruption. Regeneration of Golgi stacks at peripheral endoplasmic reticulum exit sites. *Mol. Biol. Cell* **7,** 631–650
56. Binker, M. G., Cosen-Binker, L. I., Terebiznik, M. R., Mallo, G. V., McCaw, S. E., Eskelinen, E. L., Willenborg, M., Brumell, J. H., Saftig, P., Grinstein, S., and Gray-Owen, S. D. (2007) Arrested maturation of *Neisseria*-containing phagosomes in the absence of the lysosome-associated membrane proteins, LAMP-1 and LAMP-2. *Cell Microbiol.* **9,** 2153–2166
57. Manfredi, J. J., Parness, J., and Horwitz, S. B. (1982) Taxol binds to cellular microtubules. *J. Cell Biol.* **94,** 688–696
58. Kawasaki, K., Akashi, S., Shimazu, R., Yoshida, T., Miyake, K., and Nishijima, M. (2000) Mouse toll-like receptor 4.MD-2 complex mediates lipopolysaccharide-mimetic signal transduction by Taxol. *J. Biol. Chem.* **275,** 2251–2254
59. Vasquez, R. J., Howell, B., Yvon, A. M., Wadsworth, P., and Cassimeris, L. (1997) Nanomolar concentrations of nocodazole alter microtubule dynamic instability *in vivo* and *in vitro*. *Mol. Biol. Cell* **8,** 973–985
60. Silver, K. E., and Harrison, R. E. (2011) Kinesin 5B is necessary for delivery of membrane and receptors during FcγR-mediated phagocytosis. *J. Immunol.* **186,** 816–825
61. Wiesner, C., Faix, J., Himmel, M., Bentzien, F., and Linder, S. (2010) KIF5B and KIF3A/KIF3B kinesins drive MT1-MMP surface exposure, CD44 shedding, and extracellular matrix degradation in primary macrophages. *Blood* **116,** 1559–1569
62. Nakata, T., and Hirokawa, N. (1995) Point mutation of adenosine triphosphate-binding motif generated rigor kinesin that selectively blocks anterograde lysosome membrane transport. *J. Cell Biol.* **131,** 1039–1053
63. Opdenakker, G., Van den Steen, P. E., Dubois, B., Nelissen, I., Van Coillie, E., Masure, S., Proost, P., and Van Damme, J. (2001) Gelatinase B functions as regulator and effector in leukocyte biology. *J. Leukoc. Biol.* **69,** 851–859
64. Wu, Y. I., Munshi, H. G., Sen, R., Snipas, S. J., Salvesen, G. S., Fridman, R., and Stack, M. S. (2004) Glycosylation broadens the substrate profile of membrane type 1 matrix metalloproteinase. *J. Biol. Chem.* **279,** 8278–8289
65. Nash, P. D., Opas, M., and Michalak, M. (1994) Calreticulin. Not just another calcium-binding protein. *Mol. Cell Biochem.* **135,** 71–78
66. Johnson, S., Michalak, M., Opas, M., and Eggleton, P. (2001) The ins and outs of calreticulin. From the ER lumen to the extracellular space. *Trends Cell Biol.* **11,** 122–129
67. Michalak, M., Corbett, E. F., Mesaeli, N., Nakamura, K., and Opas, M. (1999) *Biochem. J.* **344,** 281–292
68. Bu, C. H., and Pourmotabbed, T. (1995) Mechanism of activation of human neutrophil gelatinase B. Discriminating between the role of Ca^{2+} in activation and catalysis. *J. Biol. Chem.* **270,** 18563–18569
69. Millar, A. L., Pavios, N. J., Xu, J., and Zheng, M. H. (2002) Rab3D. A

regulator of exocytosis in non-neuronal cells. *Histol. Histopathol.* **17,** 929–936
70. Reed, N. A., Cai, D., Blasius, T. L., Jih, G. T., Meyhofer, E., Gaertig, J., and Verhey, K. J. (2006) Microtubule acetylation promotes kinesin-1 binding and transport. *Curr. Biol.* **16,** 2166–2172
71. Gough, P. J., Gomez, I. G., Wille, P. T., and Raines, E. W. (2006) Macrophage expression of active MMP-9 induces acute plaque disruption in apoE-deficient mice. *J. Clin. Invest.* **116,** 59–69
72. Finlay, G. A., O'Driscoll, L. R., Russell, K. J., D'Arcy, E. M., Masterson, J. B., FitzGerald, M. X., and O'Connor, C. M. (1997) Matrix metalloproteinase expression and production by alveolar macrophages in emphysema. *Am. J. Respir. Crit. Care Med.* **156,** 240–247